



Spatial Resolution of Parallel Hot-Wire Probes for Derivative Measurements

D. Ewing

Turbulence Research Laboratory, Department of Mechanical and Aerospace Engineering, State University of New York at Buffalo, Amherst, New York

H. J. Hussein

Department of Mechanical Engineering, Vanderbilt University, Nashville, Tennessee

W. K. George

Turbulence Research Laboratory, Department of Mechanical and Aerospace Engineering, State University of New York at Buffalo, Amherst, New York

■ The spatial resolution of a parallel-wire probe is studied to evaluate the effect of finite wire spacing and wire length on the measurement of turbulence derivative quantities. The study considers the measurement of velocity and temperature derivatives in an isotropic field. Different spectral models are used for each case to determine if the amount of spatial filtering is sensitive to changes in the shape of the three-dimensional spectrum that is being measured. The data demonstrate that the separation distance is the critical dimension in probe design if the wire length and separation are of comparable magnitude. The amount of spatial filtering predicted is highly sensitive to the spectral model for separation distances greater than 2–3 times the Kolmogorov length scale.

Keywords: *spatial attenuation, parallel hot wires, turbulence, thermal anemometry*

INTRODUCTION

Direct measurements of the velocity dissipation rate, scalar dissipation rate, and mean square vorticity in a turbulent flow require the determination of a number of spatial derivatives. It is common to use a difference method with a multisensor (typically hot wires) probe to directly measure the derivatives. However, the finite dimensions of the measuring device introduce spatial filtering, so it is important to understand the effect of this filtering on the measured quantity. It is evident that it is not the absolute size of the probe that is important but the size of the probe relative to the smallest scales. In this paper the dimensions of the probe are measured in terms of the smallest dynamically significant scale, the Kolmogorov length scale.

Spatial filtering of velocity derivative measurements was initially investigated by Wyngaard [1, 2] and more recently by Antonia et al. [3, 4] and others. The spatial filtering of scalar measurements was investigated by Wyngaard [5], Browne et al. [6], and Antonia and Mi [3]. Wyngaard [2] demonstrated that the spatial filtering introduced by the finite dimensions of the probe affects the measurement of the smaller turbulent scales more significantly than it affects the measurement of the larger turbulent scales. Hussein and George [7] and Champagne [8] found this to be critical for the velocity gradients because these gradients are strongly dependent on the smallest scales of motion. The same is true for the measurement of the scalar gradients.

In the previous studies (e.g., [1–6]), empirical spectral data or Pao's [9] and Corrsin's [10] spectrum functions

have primarily been used to model the turbulence. It is widely believed that the latter spectrum functions do not roll off fast enough at high wavenumbers. If so, the error due to spatial filtering is significantly overestimated. In addition, Ligrani and Bradshaw [11] noted that Wyngaard's analysis was limited in the sense that it examined only a single spectrum model whereas in real flow situations, such as a boundary layer, the nature of the turbulence may vary significantly from point to point. These issues prompted Antonia et al. [3, 4] to use direct numerical simulation measurements from a channel flow and three-dimensional spectrum functions, determined by measuring one-dimensional spectra using the isotropic relationships, to model the turbulence. They concluded that the attenuation was weakly dependent on the model of the three-dimensional spectrum. In addition, using measurements and data from direct numerical simulation for a channel flow, Antonia et al. [4] noted that the amount of attenuation increased near the wall of the channel and suggested that Wyngaard's analysis was not valid in this region because it could not predict this increase.

The objective of this paper is to examine the sensitivity of spatial filtering to changes in the spectral model in addition to the effects of the finite wire separation and wire length of the probe. To accomplish this, additional spectrum functions are used in the calculations for both the velocity and temperature derivatives. The effect of the model for high-wavenumber regions on the attenuation of the derivative measurements is examined by using Lin's [12] spectrum function for the velocity derivative calculations and Hill's [13] scalar version of the spectrum for the

Address correspondence to Dr. Daniel Ewing, 321 Jarvis Hall, SUNY at Buffalo, Amherst, New York 14260.

scalar derivative calculation. Lin's and Hill's spectrum functions roll off more quickly at the higher wavenumbers than Pao's and Corrsin's spectrum functions. In addition, a composite spectrum [14] is added in the velocity derivative calculations to consider the effects of finite Reynolds number and the energy-containing range on the derivative measurements.

THE ATTENUATION OF VELOCITY DERIVATIVE MEASUREMENTS

To determine how the separation distance affects the velocity derivative measured with a parallel-probe hot wire (shown in Fig. 1), the two wires are initially modeled as zero-length wires, so there is no spatial averaging due to finite wire length. Finite-length effects are added later, and the attenuation of the derivative measurement is calculated as a function of wire length for two different separation distances. Calculations are carried out for all of the spectral models to determine the sensitivity of the error to the spectral model utilized.

Filtering Due to Finite Separations

The zero-length parallel-wire probe measures the velocity at two points in the field, which can be labeled \mathbf{x}_a and \mathbf{x}_b (for finite-length wire, the points \mathbf{x}_a and \mathbf{x}_b correspond to the center of each wire in Fig. 1). The velocity derivative is estimated by taking the difference in velocities at the two points and dividing this by the distance between the points. In the limit of zero separation, this is the definition of the exact derivative at a point. What follows is a mathematical derivation of this derivative estimate in Fourier space, which parallels the derivation of Wyngaard [2].

For a homogeneous random field, the velocity can be represented, using the notation of George and Lumley [16], by its inverse Fourier transform (in the sense of generalized functions [15]),

$$u(\mathbf{x}) = \int e^{i\mathbf{k} \cdot \mathbf{x}} \hat{u}(\mathbf{k}) d\mathbf{k}, \quad (1)$$

where \mathbf{k} is the wavenumber vector. The current analysis assumes that Taylor's frozen field hypothesis is valid at all wavenumbers of the turbulence. Thus the temporal variations measured by the hot wire are the result of a frozen homogeneous field being convected over the hot wires with a fixed mean convection velocity U .

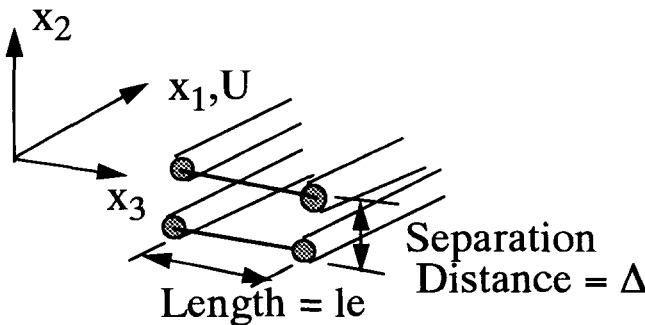


Figure 1. Geometry of the parallel-wire probe.

In the current analysis, it is assumed that the hot wires measure only the streamwise component of velocity at the two points; the effect of cross-flow contamination is neglected. (Other velocity components and different wire configurations will be considered in a subsequent paper.) The difference between the velocities at these two points in space, \mathbf{x}_a and \mathbf{x}_b , is

$$[u_1(\mathbf{x}_a) - u_1(\mathbf{x}_b)] = \int \hat{u}_1(\mathbf{k}) [e^{i\mathbf{k} \cdot \mathbf{x}_a} - e^{i\mathbf{k} \cdot \mathbf{x}_b}] d\mathbf{k}. \quad (2)$$

Dividing this velocity difference by the separation distance between the points yields an estimate of the derivative. Using this expression, it is possible to calculate the mean square of the estimated velocity derivative for a finite separation as

$$\begin{aligned} & \frac{[u_1(\mathbf{x}_a) - u_1(\mathbf{x}_b)]^2}{|\mathbf{x}_a - \mathbf{x}_b|^2} \\ &= \frac{1}{|\mathbf{x}_a - \mathbf{x}_b|^2} \iint [e^{i\mathbf{k} \cdot \mathbf{x}_a} - e^{i\mathbf{k} \cdot \mathbf{x}_b}] [e^{-i\mathbf{k}' \cdot \mathbf{x}_a} - e^{-i\mathbf{k}' \cdot \mathbf{x}_b}] \\ & \quad \times \hat{u}_1(\mathbf{k}) \hat{u}_1^*(\mathbf{k}') d\mathbf{k} d\mathbf{k}'. \end{aligned} \quad (3)$$

For a homogeneous field, nonoverlapping Fourier coefficients are uncorrelated [16], so that

$$\hat{u}_1(\mathbf{k}) \hat{u}_1^*(\mathbf{k}') d\mathbf{k} d\mathbf{k}' = \Phi_{11}(\mathbf{k}) \delta(\mathbf{k}' - \mathbf{k}) d\mathbf{k} d\mathbf{k}'. \quad (4)$$

Therefore the equation for the measured derivative becomes

$$\begin{aligned} & \frac{[u_1(\mathbf{x}_a) - u_1(\mathbf{x}_b)]^2}{|\mathbf{x}_a - \mathbf{x}_b|^2} \\ &= \int \Phi_{11}(\mathbf{k}) \frac{\{2 - 2 \cos[\mathbf{k} \cdot (\mathbf{x}_a - \mathbf{x}_b)]\}}{|\mathbf{x}_a - \mathbf{x}_b|^2} d\mathbf{k}. \end{aligned} \quad (5)$$

This expression is valid for an arbitrary separation direction. Hereafter this study considers only probes with wires separated in the x_2 coordinate direction, which is normal to the mean flow direction. Since the three-dimensional velocity spectra examined in this study are isotropic, this derivative is equivalent to the measured derivative in any direction normal to the flow. In the remaining portion of the paper Δ is used to represent the magnitude of the separation distance between the wires, $|\mathbf{x}_a - \mathbf{x}_b|$.

The exact mean square derivative (i.e., zero separation limit) is given by [17]

$$\left(\frac{du_1}{dx_2} \right)^2 = \int (k_2)^2 \Phi_{11}(\mathbf{k}) d\mathbf{k}. \quad (6)$$

If the term multiplying the three-dimensional velocity spectrum in Eq. (5) is Taylor expanded about $k_2 \Delta = 0$, it is easy to see that the leading term of the expansion multiplied by the three-dimensional spectrum is equal to Eq. (6), that is,

$$\frac{1 - \cos(k_2 \Delta)}{\Delta^2} = (k_2)^2 \left[1 - \frac{(k_2 \Delta)^2}{12} + \dots \right]. \quad (7)$$

Therefore Eqs. (5) and (6) are equal in the limit of zero separation distance. Comparing the results for finite sepa-

ration distances yields the attenuation of the measured derivative due to the finite separation of the hot wires.

Velocity Spectrum

The three-dimensional velocity spectrum Φ_{ij} for a homogeneous flow is defined as the three-dimensional Fourier transform of the two-point velocity correlation; that is,

$$\Phi_{ij}(\mathbf{k}) = \frac{1}{8\pi^3} \int \overline{u_i(\mathbf{x})u_j(\mathbf{x} + \mathbf{r})} e^{i(\mathbf{k} \cdot \mathbf{r})} d\mathbf{r}, \quad (8)$$

where u_i are components of the velocity vector $\mathbf{u} = (u_1, u_2, u_3)$ and $\mathbf{k} = (k_1, k_2, k_3)$ is the wavenumber vector. The three-dimensional spectrum can be defined in terms of the three-dimensional spectrum function (also referred to as the spectrum function), $E(k)$, which is given by [18]

$$E(k) = \frac{1}{2} \int \int_{|\mathbf{k}|=k} \Phi_{ii}(\mathbf{k}) d\sigma(\mathbf{k}), \quad (9)$$

where k is the magnitude of the wavenumber \mathbf{k} and the integration is carried out over spherical shells of radius k in wavenumber space. The three-dimensional spectrum for isotropic turbulence is related to $E(k)$ by

$$\Phi_{ij} = \frac{E(k)}{4\pi k^4} (k^2 \delta_{ij} - k_i k_j). \quad (10)$$

The models of the spectrum function used in the current analysis are shown in Fig. 2. Pao's [9] model for the three-dimensional spectrum function is given by

$$\tilde{E}(\tilde{k}) = \alpha \tilde{k}^{-5/3} \exp \left[-\frac{3}{2} \alpha \tilde{k}^{4/3} \right], \quad (11)$$

where $\tilde{k} = k\eta$ and $\tilde{E}(\tilde{k}) = E(k)/u_k^2 \eta$ are the wavenumber and spectrum function nondimensionalized by the Kolmogorov length scale $\eta = (\nu^3/\varepsilon)^{1/4}$ and the Kolmogorov velocity scale $u_k = (\nu \varepsilon)^{1/4}$, where ν is the kinematic viscosity of the fluid and ε is the dissipation per unit mass. α is the Kolmogorov constant, and it is chosen as 1.6 in the current analysis, which is within the range of accepted values.

Pao's spectrum is known to be physically unrealistic in the viscous dissipation range (approximately $\tilde{k} > 0.1$), and it has a tendency to overestimate the energy in that region (see [19]). A second model that rolls off faster in this region was proposed by Lin [13] and is given by

$$\tilde{E}(\tilde{k}) = \alpha (\tilde{k}^{-5/3} + \tilde{k}^{-1}) \exp \left[-\alpha \left(\frac{3}{2} \tilde{k}^{4/3} + \tilde{k}^2 \right) \right]. \quad (12)$$

Three different values of α are chosen in this study for Lin's spectrum—1.5, 1.65, and 1.8—to determine if the

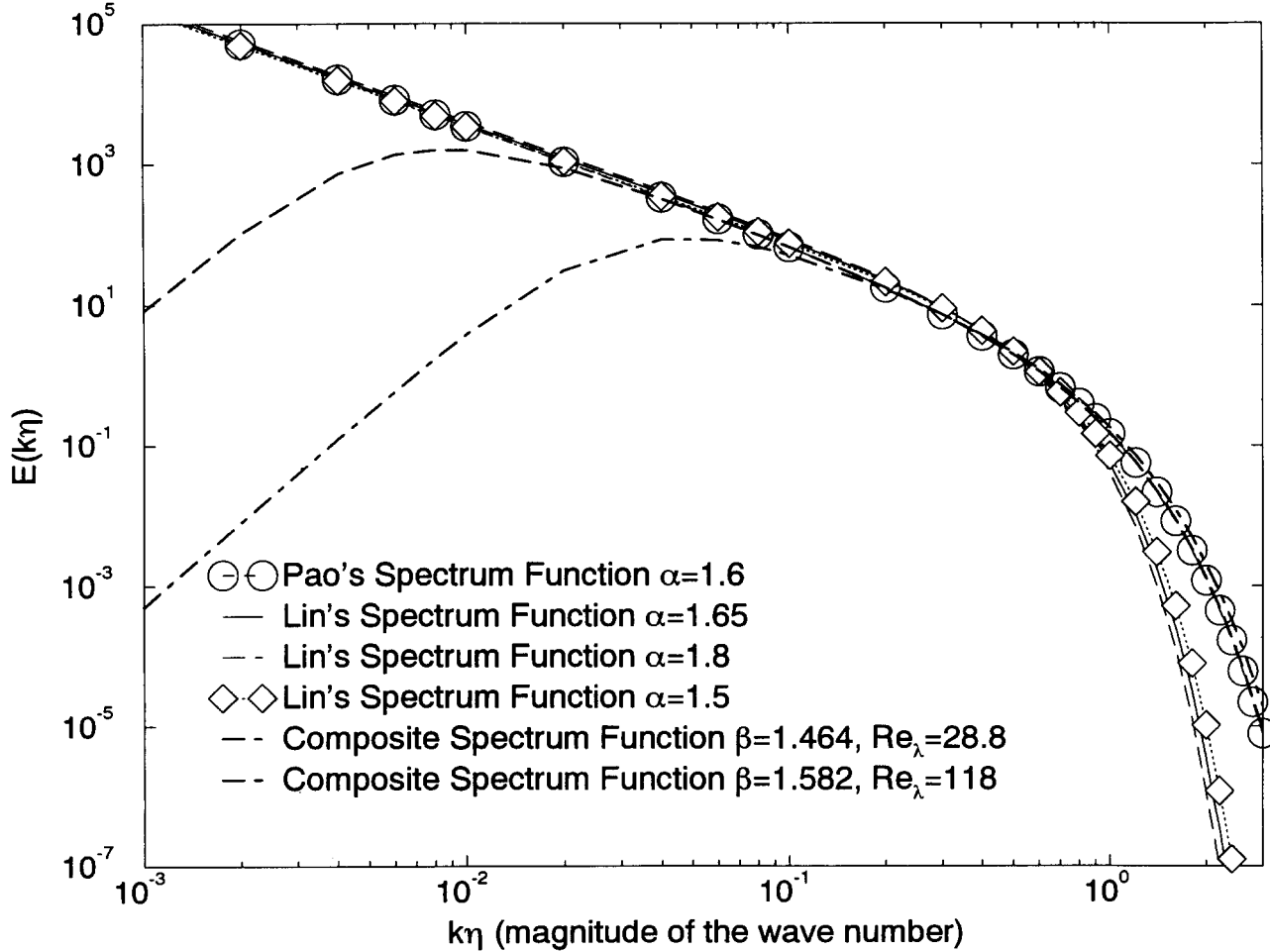


Figure 2. Velocity spectrum functions used to model the three-dimensional spectrum.

amount of spatial attenuation is sensitive to the choice of this quantity.

The previous spectral models are infinite Reynolds number models of the equilibrium range of turbulence, so they do not include a model of the energy-containing eddies. To examine the effect that the model of energy-containing eddies has on the measurement of the velocity derivative, a composite spectrum suggested by Hellend et al. (see [19]) is included. The derivation of the equations for this composite model is included in Appendix I. The spectral model combines von Karman's [20] and Pao's [9] spectra and is given by

$$\tilde{E}(\tilde{k}) = \alpha \left(\frac{L}{\eta} \right)^{5/3} \frac{[\tilde{k}(L/\eta)]^4}{[1 + \{\tilde{k}(L/\eta)\}^2]^{17/6}} \exp \left[-\frac{3}{2} \beta \tilde{k}^{4/3} \right], \quad (13)$$

where α is a model constant defined to be 1.6 in this analysis and L is a length scale characteristic of the energy-containing eddies. For a given choice of L/η it is possible to calculate the other model constant β by satisfying the dissipation equation ([18])

$$\varepsilon = 2\nu \int_0^\infty k^2 E(k) dk. \quad (14)$$

The Reynolds number for the spectrum can be characterized by the turbulence Reynolds number based on the Taylor microscale λ ; that is,

$$Re_\lambda = u\lambda/\nu, \quad (15)$$

where $u^2 = \overline{(u_i u_i)}/3$. For isotropic turbulence, the relationship between the turbulence Reynolds number based on the Taylor microscale and the spectrum function is given by

$$Re_\lambda = \left(\frac{20}{3} \right)^{1/2} \int_0^\infty \tilde{E}(\tilde{k}) d\tilde{k}. \quad (16)$$

Therefore, once a value of L/η is chosen, the corresponding value of β can be calculated using Eq. (14), and the turbulence Reynolds number based on the Taylor microscale can be determined from Eq. (16). The value of the parameters L/η , β , and Re_λ for the spectrum functions used in this analysis are included in Table 1.

The one-dimensional spectrum of the turbulence, $F_{ij}^1(k_1)$, is the spectrum usually available to the experimenter. The one-dimensional spectrum is related to the three-dimensional spectrum Φ_{ij} by

$$F_{ij}^1(k_1) = \int \int \Phi_{ij}(\mathbf{k}) dk_2 dk_3. \quad (17)$$

The one-dimensional spectra, normalized by Kolmogorov variables $\tilde{F}_{11}^1 = F_{11}^1/u_k^2 \eta$ corresponding to the spectrum functions above are illustrated in Fig. 3. The spectra in this figure are the positive wavenumber portion of the

whole line spectrum. They are representative of the whole line spectrum, since the one-dimensional spectrum is an even function for $i = j$. Note that there are substantial differences between the one-dimensional spectra for Lin's function and the one-dimensional spectrum for Pao's function. It is clear that the one-dimensional spectra of the models that incorporate Pao's spectrum function to model the high-wavenumber region do not roll off as quickly as the models that incorporate Lin's spectrum function in this region. In addition, it should be noted that the one-dimensional spectrum of the composite spectrum levels off in the low-wavenumber region in a manner that is consistent with measured one-dimensional spectra while the one-dimensional spectra of the other two models continue to rise.

Attenuation of the Mean Square Derivative

Figure 4 illustrates the attenuation that occurs in the measured derivatives for the two different infinite Reynolds number models of the equilibrium range. The values of the measured derivatives have been normalized by the value of the exact derivative (i.e., the derivative that would be measured by a probe of zero dimension) to illustrate the relative attenuation. There are several important points to note from this graph. The relative error that occurs in the measured derivative is strongly dependent on the choice of the model of the equilibrium range of the three-dimensional spectrum function. The error in the normalized derivative measurement for Lin's spectrum is significantly less than the error for Pao's spectrum. The faster rolloff of Lin's spectrum function in the dissipation region is the direct cause of this reduction. Finally, Lin's model distributes relatively more of the spectral density of the three-dimensional derivative spectrum at smaller values of k_2 where the attenuation caused by the measuring technique is smaller. This reduces the amount of attenuation in the mean square derivative measurement.

It is clear from this analysis that the amount of attenuation is sensitive to the shape of the velocity spectrum function in the high-wavenumber region and the sensitivity increases as the separation distance between the probes increases. The three curves in Fig. 4 that use Lin's model demonstrate that the attenuation is not strongly dependent on the parameter α in this model. Figure 4 also includes data reported by Antonia et al. [4] that were calculated using data from a direct numerical simulation of a fully developed channel flow. The instantaneous velocity field at the centerline of the channel was used to estimate the instantaneous velocity derivative with a difference technique for various separation distances. The correct derivative for zero separation was estimated using Chebychev polynomials. The relative attenuation of the mean square derivative due to the finite separation of the points is the ratio of the variance of these two quantities. The data from the direct numerical simulation are in good agreement with the curves calculated using Lin's spectrum function, indicating that this spectrum function provides a reasonable estimate of the error in the derivative measurements.

Figure 5 illustrates that the amount of attenuation that occurs in the measured derivative is dependent on the

Table 1

L / η	β	Re_λ
31.6	1.464	28.8
178	1.582	118

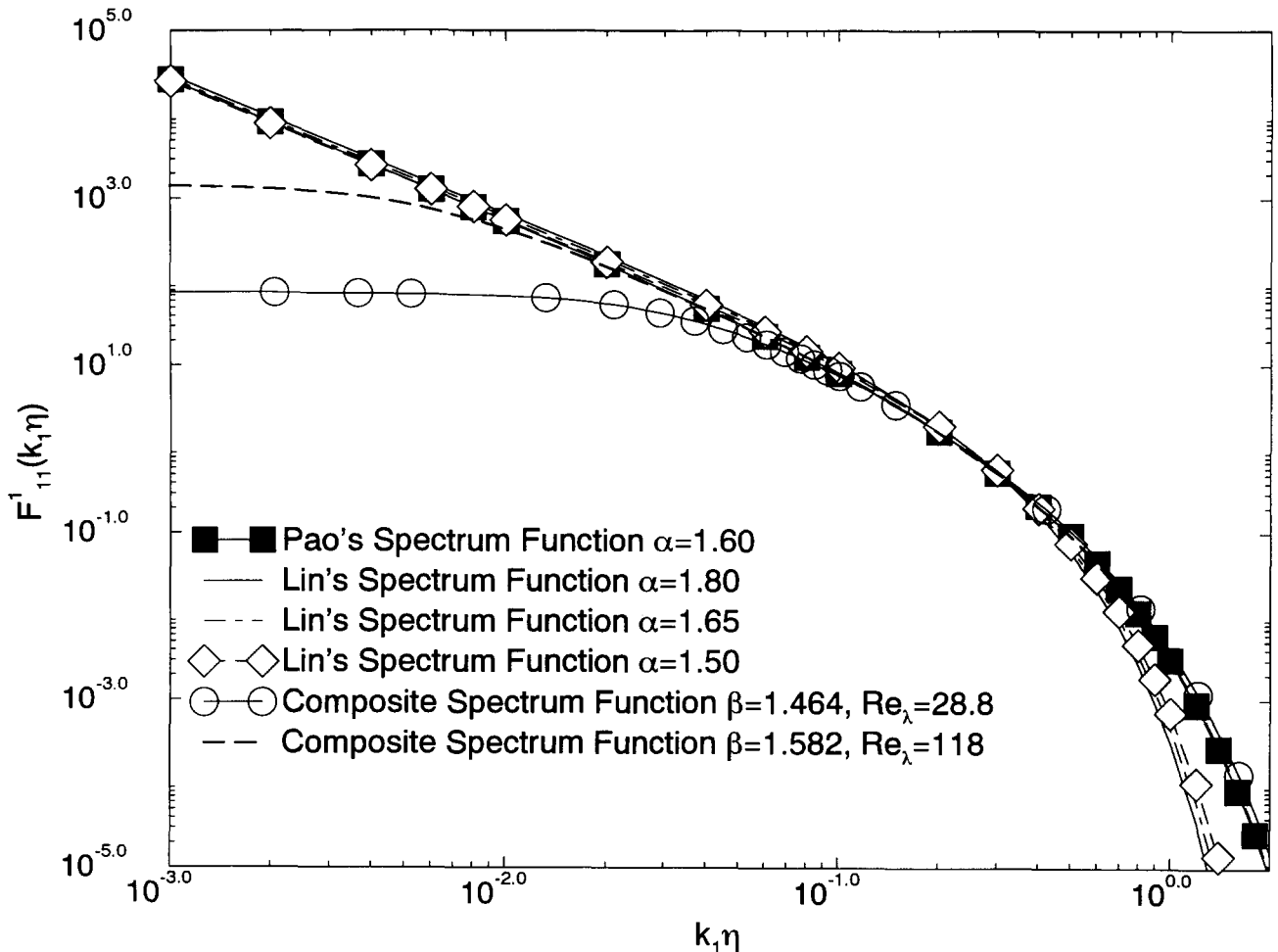


Figure 3. Comparison of the one-dimensional velocity spectra.

model of the low-wavenumber region when the Reynolds number is small. For the cases considered in the figure, the value of β is less than the value of α , so the spectrum functions roll off more slowly than Pao's function with the value of α in the exponential rolloff term. To compensate for this effect, the attenuation that occurs for Pao's spectrum function with α equal to each of the values of β is included as a reference. For the larger Reynolds numbers, such as $Re_\lambda = 118$, the attenuation of the measured derivative calculated using the composite spectrum function is not significantly different from the attenuation that occurs for Pao's spectrum function. For smaller Reynolds numbers, such as $Re_\lambda = 28.8$, the attenuation of the measured derivative is dependent on the model of the low-wavenumber region. Decreasing the Reynolds number decreases the ratio of the characteristic length scale of the energy-containing eddies and the Kolmogorov length scale and causes the three-dimensional derivative spectrum to extend over a smaller region in wavenumber space. As the region shrinks, the effect of the spatial attenuation will extend over an increasing portion of the three-dimensional spectrum if the separation distance between the wires in the probe is held at a fixed value relative to the Kolmogorov length scale (which occurs in the figures). This causes the relative attenuation of the measured

derivative to increase as Re decreases. In addition, Fig. 5 demonstrates that the sensitivity of the attenuation to the model of the low-wavenumber region increases as the separation distance between the wires in the probe increases. It is important to note that Taylor's frozen field hypothesis and the assumption of isotropy are not valid for the large-scale motions in high turbulence intensity flows. Therefore, the results for the very low Reynolds number case yields valuable qualitative information, but the results may not be quantitatively accurate because of these failures.

The experimental measurements from Fig. 7 of Klewicki and Falco [22] have also been included in Fig. 5. Klewicki and Falco carried out measurements in a boundary layer at $y^+ = 38$ and 58 ($y^+ = yu_\tau/\nu$, where u_τ is the friction velocity) using two sets of wires centered on a single point. One set of wires had a fixed separation distance of approximately 1 times the Kolmogorov length scale while the spacing of the second wire was varied. They normalized the root mean square (rms) derivative measured with the outer wire by the rms derivative measured using the inner wire. The data from this figure have been processed to correspond to the quantity plotted in Fig. 5. The experimental data do not agree with the calculated values at the smallest separation distances, but for larger separations

there is good agreement. It is interesting to note that the attenuation in the experimental data seems to demonstrate a dependency on the location in the boundary layer, indicating that the attenuation is dependent on Re since the turbulence Reynolds number in the boundary layer increases with y^+ . Antonia et al. [4] also reported this phenomenon for derivative measurements near the wall of a channel flow. For larger separation distances (i.e., $\Delta > 4\eta$), they noticed that the amount of attenuation increased significantly as the probe was moved closer to the wall when the ratio of the separation distance of the probe and the local Kolmogorov length scale was constant. This is the outcome that the analysis using the low Reynolds number spectrum predicts.

The analysis of the probe spatial filtering demonstrates that the separation distance should be minimized to minimize the error introduced by the transducer. In real experiments there is a lower limit to this separation due to the noise in the experimental setup [3]. This problem is addressed further in a later section.

Inferring Attenuation from One-Dimensional Spectra

Normally the only spectral measurements that an experimentalist will have available are one-dimensional spectra

of the quantity that is measured. The measured one-dimensional spectrum of the derivative of the u_1 component with respect to x_2 , $F_{1,2;1,2}^1$, can be related to a measured three-dimensional spectrum by

$$F_{1,2;1,2}^1(k_1)_m = \frac{2}{\Delta^2} \int \int \Phi_{11}(\mathbf{k}) [1 - \cos(k_2 \Delta)] dk_2 dk_3, \quad (18)$$

where the term inside the integration is the spatially filtered three-dimensional spectrum. This spectrum was calculated for a number of separation distances using Lin's spectrum with $\alpha = 1.65$.

The spectra are illustrated in Fig. 6 on a traditional log-log plot together with the exact one-dimensional spectrum of the derivative

$$F_{1,2;1,2}^1(k_1)_{ext} = \int \int (k_2)^2 \Phi_{11}(\mathbf{k}) dk_2 dk_3. \quad (19)$$

It is clear from this figure that the measured one-dimensional spectra are attenuated at high wavenumbers and that the amount of attenuation at any particular wavenumber k_1 increases as the separation distance increases.

A question that can be asked is whether this plot of the one-dimensional spectrum yields a proper picture of the

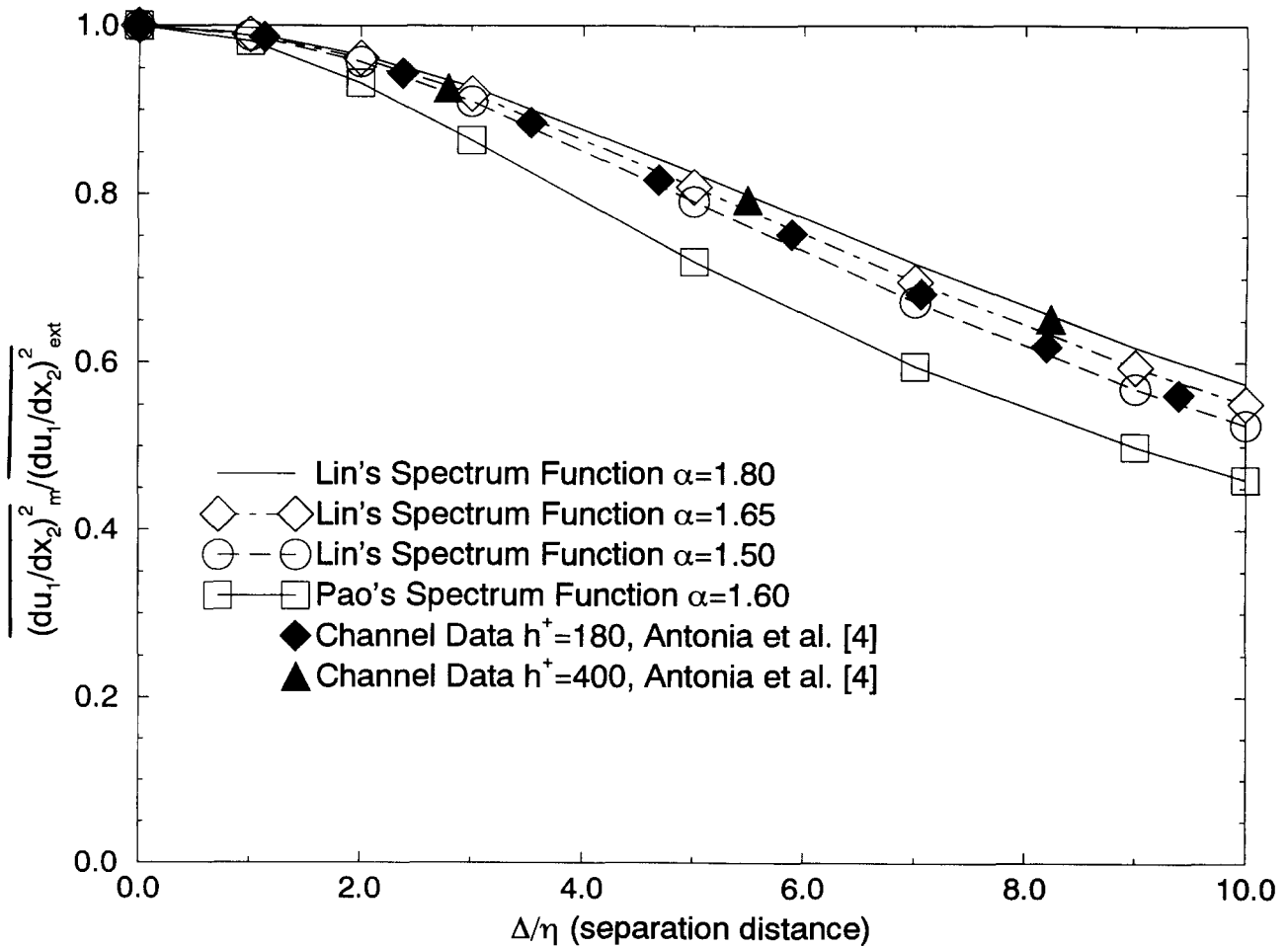


Figure 4. Attenuation of velocity derivative measurements due to the finite separation of zero-length wires for the high-wavenumber models.

filtering process and whether it is possible to determine a cutoff frequency from this type of figure. To answer this question it is necessary to look at the three-dimensional spectra of the measured derivative and the exact derivative. This is straightforward when it is recognized that Eqs. (5) and (6) are integrations of the measured and exact three-dimensional derivative spectra over the wave space. Therefore the normalized attenuation that occurs in the three-dimensional wavenumber space is the ratio of the measured and exact three-dimensional spectra

$$\frac{\text{Measured}}{\text{Unattenuated}} = \frac{2(1 - \cos[k_2\Delta])}{\Delta^2(k_2)^2}$$

$$= 1 - \frac{1}{12}(k_2\Delta)^2 + \dots; \quad (20)$$

where the final set of terms in the equation are the Taylor expansion of the ratio about $k_2 = 0$.

There are a number of important observations that can be made from this ratio of the measured three-dimensional derivative spectrum to the exact three-dimensional derivative spectrum for $\partial u_1 / \partial x_2$. The attenuation of the three-dimensional spectrum is a function of k_2 only and is independent of k_1 and k_3 . Therefore, the spatial filtering

due to the finite separation is equivalent to applying a filter to the exact three-dimensional spectrum that filters only the three-dimensional spectrum function in one direction. The leading order error term of the Taylor series for this ratio is $(k_2\Delta)^2/12$ for $k_2\Delta < 1$, so the attenuation of the measured three-dimensional spectrum is small unless k_2 is on order of $1/\Delta$. Since the filtering process is a function of only k_2 , the cutoff wavenumber (e.g., the wavenumber where the local attenuation level is a certain percentage of the actual value) should be a value k_2 that is dependent on only the definition of the cutoff frequency and the dimensions of the probe relative to the scales in the flow.

The value of the one-dimensional spectrum for a given value of k_1 is determined by integrating all of the spectral density in wavenumbers k with a streamwise component equal to k_1 [see, e.g., eqs. (14) and (15), where the integration is over k_2 and k_3 with fixed k_1]. This leads to the aliasing problem described by Tennekes and Lumley [21], which arises because a function of the vector k is mapped onto a function of the scalar k_1 . As a result, the one-dimensional spectrum at k_1 is aliased from higher wavenumbers $k > k_1$ [i.e., on a plane of fixed k_1 , the wavenumber $k = (k_1 k_1 + k_2 k_2 + k_3 k_3)^{1/2} > k_1$]. In addition, since the finite dimensions of the probe filter the

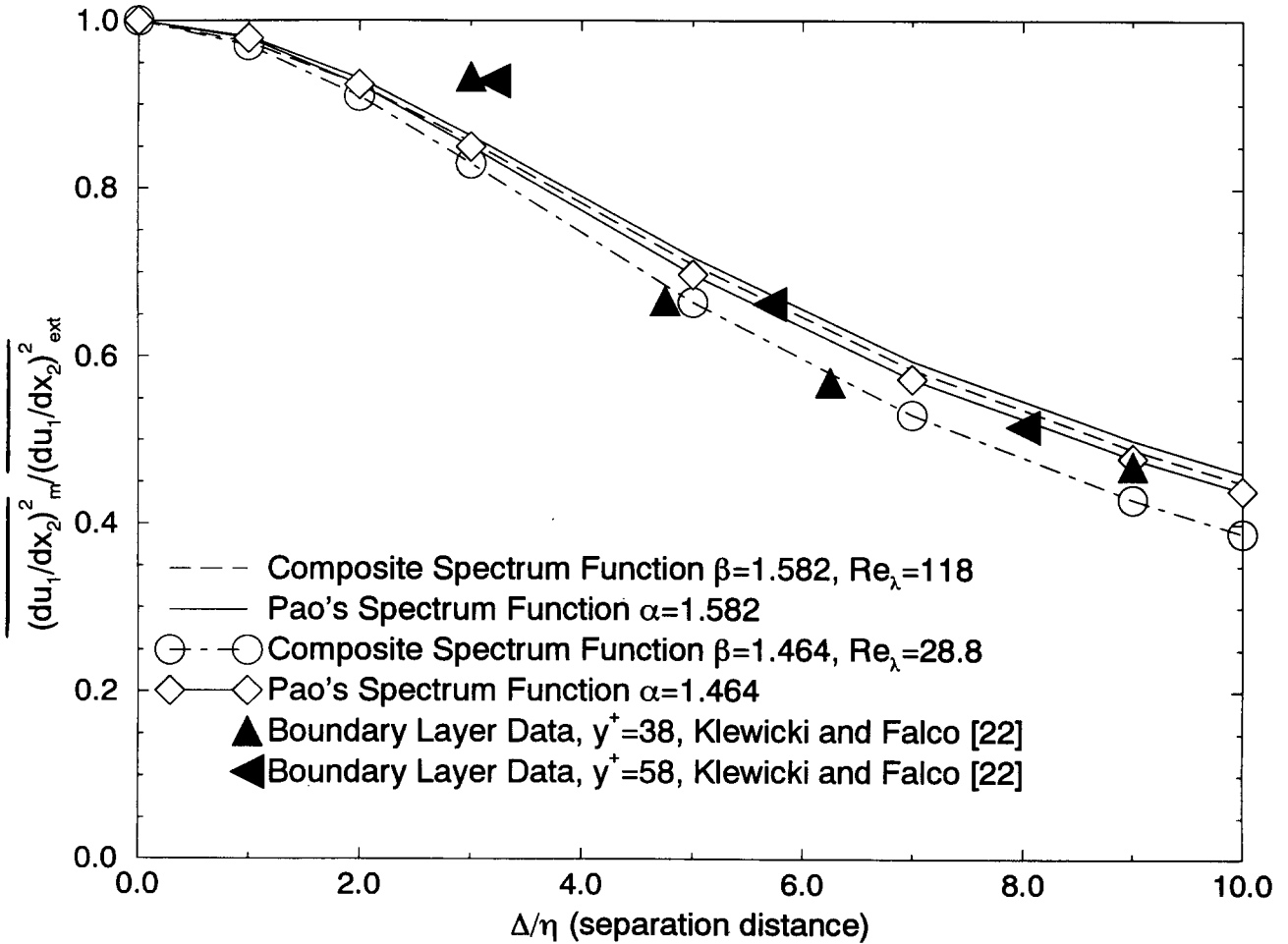


Figure 5. Attenuation of velocity derivative measurements due to the finite separation of zero-length wires for the finite Reynolds number models.

three-dimensional spectrum as a function k_2 , the energy that is being aliased from the higher wavenumbers will be attenuated by different amounts. Therefore, the attenuation of the one-dimensional spectrum occurring at any value of k_1 will depend not only on the dimensions of the probe and the definition of the cutoff frequency, but also on the particular three-dimensional spectrum that is being measured because it is a function of the way in which the spectral density is distributed on the plane of fixed k_1 (i.e., how much of the relative spectral density occurs in regions where the attenuation is large). This point is illustrated in Fig. 7, where the ratio of the measured one-dimensional spectrum to the exact one-dimensional spectrum is plotted as a function of the wavenumber k_1 for Lin's spectrum function and the composite spectrum function with a Reynolds number of 28.8 (analogous to the plot Wyngaard [2] used to illustrate this point for a vorticity probe).

Figure 7 illustrates that the attenuation of the one-dimensional spectrum occurs over a large range of the nondimensional wavenumber and increases as the wavenumber increases. A close examination of the log-log plot for the attenuated one-dimensional spectra (i.e., Fig. 6) reveals that there is attenuation of the one-dimensional spectra at the low value of $k_1\eta$, but it is easy to overlook

this in a log-log format and misinterpret the nature of the attenuation process. In addition, the figure demonstrates that the amount of attenuation that is occurring in the one-dimensional spectrum is dependent on the three-dimensional spectrum of the turbulence. Thus, it is in general not possible to calculate a proper cutoff frequency using the conventional one-dimensional spectrum of the derivative in the x_2 direction, which is independent of the three-dimensional spectrum that is being measured.

Filtering Due to Finite Wire Length

In reality, wires have a finite length, which increases the attenuation of the measured velocity derivative. Wyngaard [1] derived an expression for the attenuation of velocity measurements due to the finite length of a single wire. If the temperature of the wire is approximately constant along its length and the turbulence intensity is small, the effect of the wire can be closely estimated by line averaging the velocity along the length of the wire,

$$\bar{u}(x_a) = \frac{1}{|l|} \int_{x_a - 1/2}^{x_a + 1/2} u(s) ds, \quad (21)$$

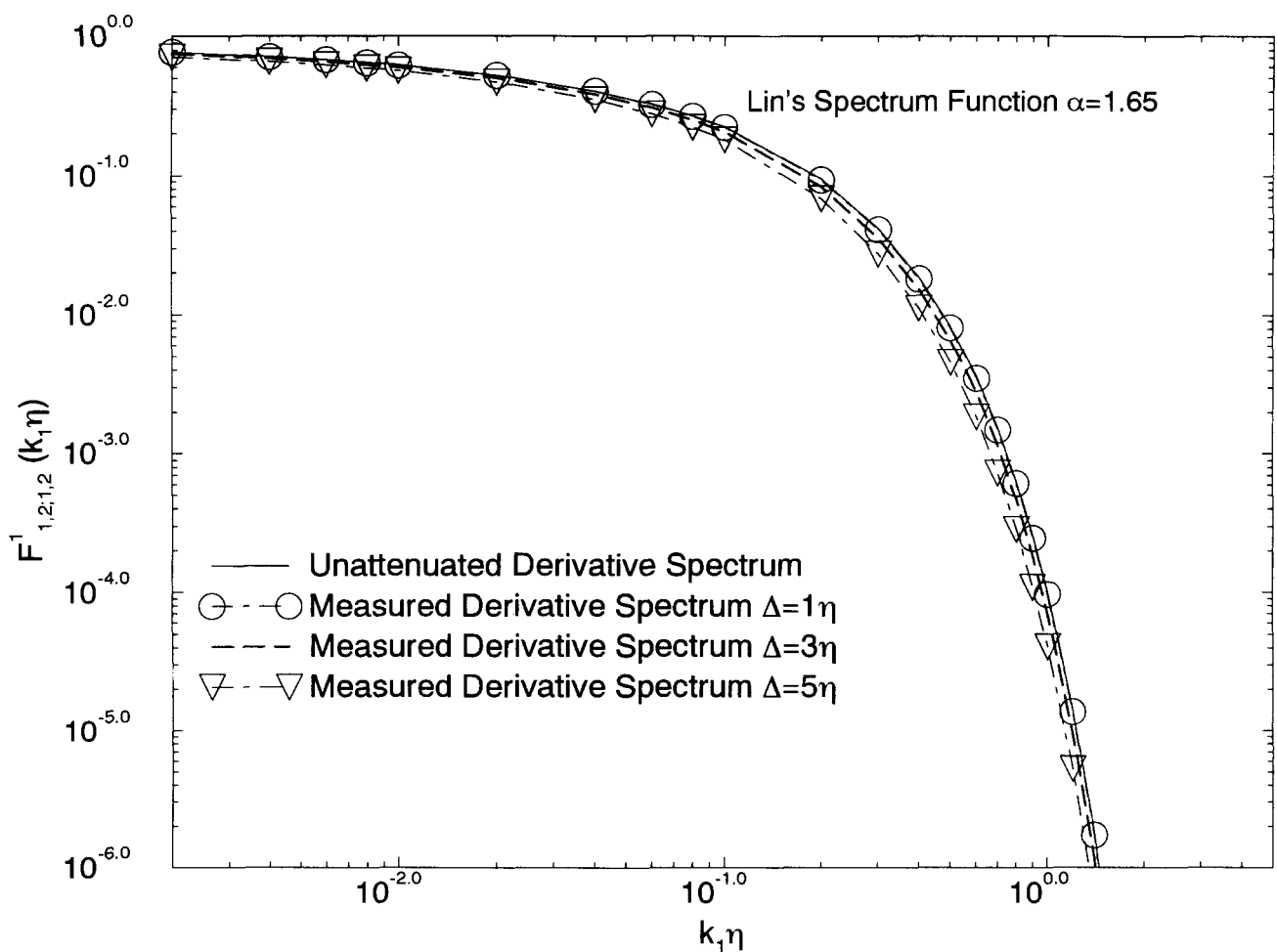


Figure 6. Attenuation of the one-dimensional velocity derivative spectra measured by finitely separated zero-length parallel wires, Lin's spectrum function.

where \mathbf{x}_a is the midpoint of the wire, \mathbf{l} is a vector parallel to the wire, and \underline{u} is used to denote the velocity measured by the wire. The integration is a line integration that is parameterized to follow the wire. The expression for the inverse Fourier transform (in the sense of generalized functions) for the measured velocity becomes [1]

$$\underline{u}(\mathbf{x}_a) = \int e^{i\mathbf{k} \cdot \mathbf{x}_a} \hat{u}(\mathbf{k}) \frac{\sin(\mathbf{k} \cdot \mathbf{l}/2)}{\mathbf{k} \cdot \mathbf{l}/2} d\mathbf{k}. \quad (22)$$

In this study the two wires are parallel to each other, so the vectors along the wires are parallel in space. As a result, the expression for the mean square measured derivative with the finite-length wires requires the addition of one extra factor to the integral in Eq. (5) [2]

$$\begin{aligned} & \frac{[\underline{u}(\mathbf{x}_a) - \underline{u}(\mathbf{x}_b)]^2}{|\mathbf{x}_a - \mathbf{x}_b|^2} \\ &= \frac{1}{|\mathbf{x}_a - \mathbf{x}_b|^2} \int \Phi_{11}(\mathbf{k}) \{2 - 2 \cos[\mathbf{k} \cdot (\mathbf{x}_a - \mathbf{x}_b)]\} \\ & \quad \times \left(\frac{\sin(\mathbf{k} \cdot \mathbf{l}/2)}{\mathbf{k} \cdot \mathbf{l}/2} \right)^2 d\mathbf{k}. \end{aligned} \quad (23)$$

The symbol l_e is used to represent the physical length of the wire. For the geometry analyzed in this paper, the wavenumber parallel to the wire is k_3 . Therefore the amount of filtering that occurs at any point in the measured three-dimensional spectrum due to the averaging along the length of the wire depends only on the value of k_3 and the length of the wire. The normalized attenuation of the three-dimensional spectrum, at any wavenumber, due to the finite wire separation and wire length is

$$\frac{\text{Measured}}{\text{Exact}} = \frac{2[1 - \cos(k_2 \Delta)]}{\Delta^2 (k_2)^2} \left(\frac{\sin(k_3 l_e / 2)}{k_3 l_e / 2} \right)^2, \quad (24)$$

where the first portion of the term is the filter due to the finite separation and the term in large parentheses is the filter due to the finite length of the wire.

A physical interpretation of the filtering due to the finite length of the wire can be illustrated quite easily using the diagram in Fig. 8. Wire 1 in this figure has disturbances (the solid lines represent the peaks of the disturbances) with only one wavenumber component k_1 moving across a wire. It is clear that the wave disturbances cause the velocity at each point on the wire to vary uniformly and the averaging by the wire will not affect the measured value of the amplitude. Wire 2 represents the

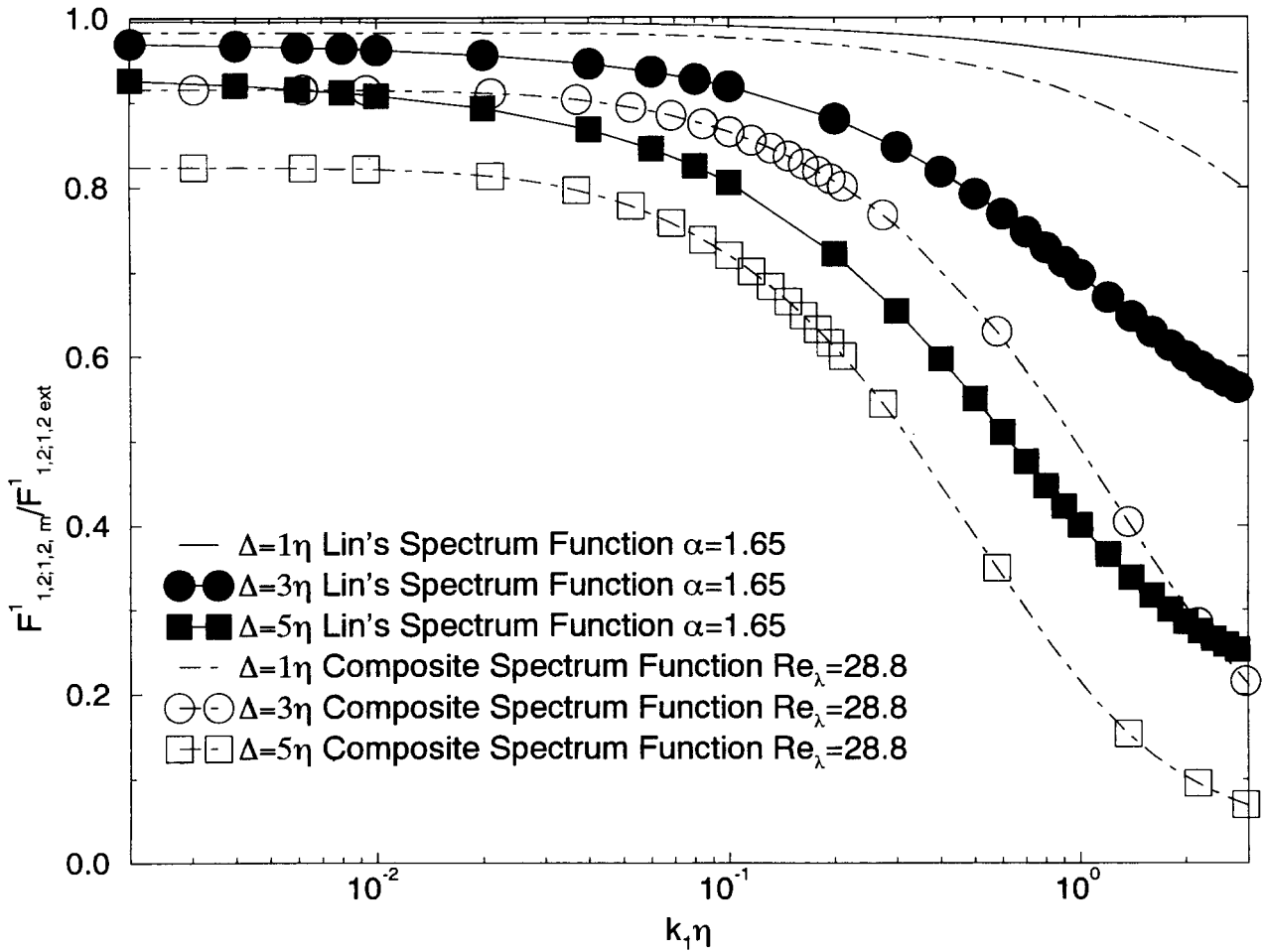


Figure 7. Normalized attenuation of the one-dimensional velocity derivative spectra measured by finitely separated zero-length parallel wires.

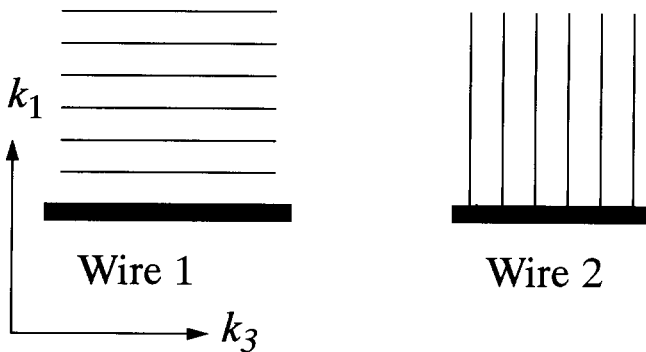


Figure 8. Illustration of the effect of line averaging on disturbances with different wavenumbers.

case of a disturbance with only one component k_3 being convected across the wire. In this case there are many oscillations of the velocity along the length of the wire and the averaging effect of the wire will result in a measured amplitude that is much smaller than the amplitude of the wave in the flow. Of course, in turbulence most of the disturbances have all three wavenumber components, but the principle is the same: the amount of attenuation that

occurs in the three-dimensional spectrum due to the finite wire length is a function of the wavenumber parallel to the direction of the wire, k_3 in this case.

Figure 9 demonstrates the effect of using finite-length wires in a probe for separation distances of 1 and 3 times the Kolmogorov length scale. This figure demonstrates that the additional attenuation that occurs in the measured derivative due to the finite length of the wires is dependent on the model of the spectrum of the high-wavenumber region, with Pao's spectral model yielding the higher error, as expected. For Lin's spectrum function, probes with small wire lengths of 3–4 times the Kolmogorov length scale add only 2–3% additional error. It is clear that if the wire length and the wire separation are approximately equal (for this geometry and these spectral models), the separation distance is the critical dimension in determining the amount of attenuation. It is possible to understand why the wire length adds a small amount of additional attenuation for these models. Recall that differentiating with respect to x_2 is equivalent to multiplying the three-dimensional velocity spectrum by k_2^2 . This has a tendency to concentrate the spectral density of the three-dimensional derivative spectrum in the region where k_2 is large. Therefore a finite-length wire normal to the separation distance does not attenuate the spectrum directly

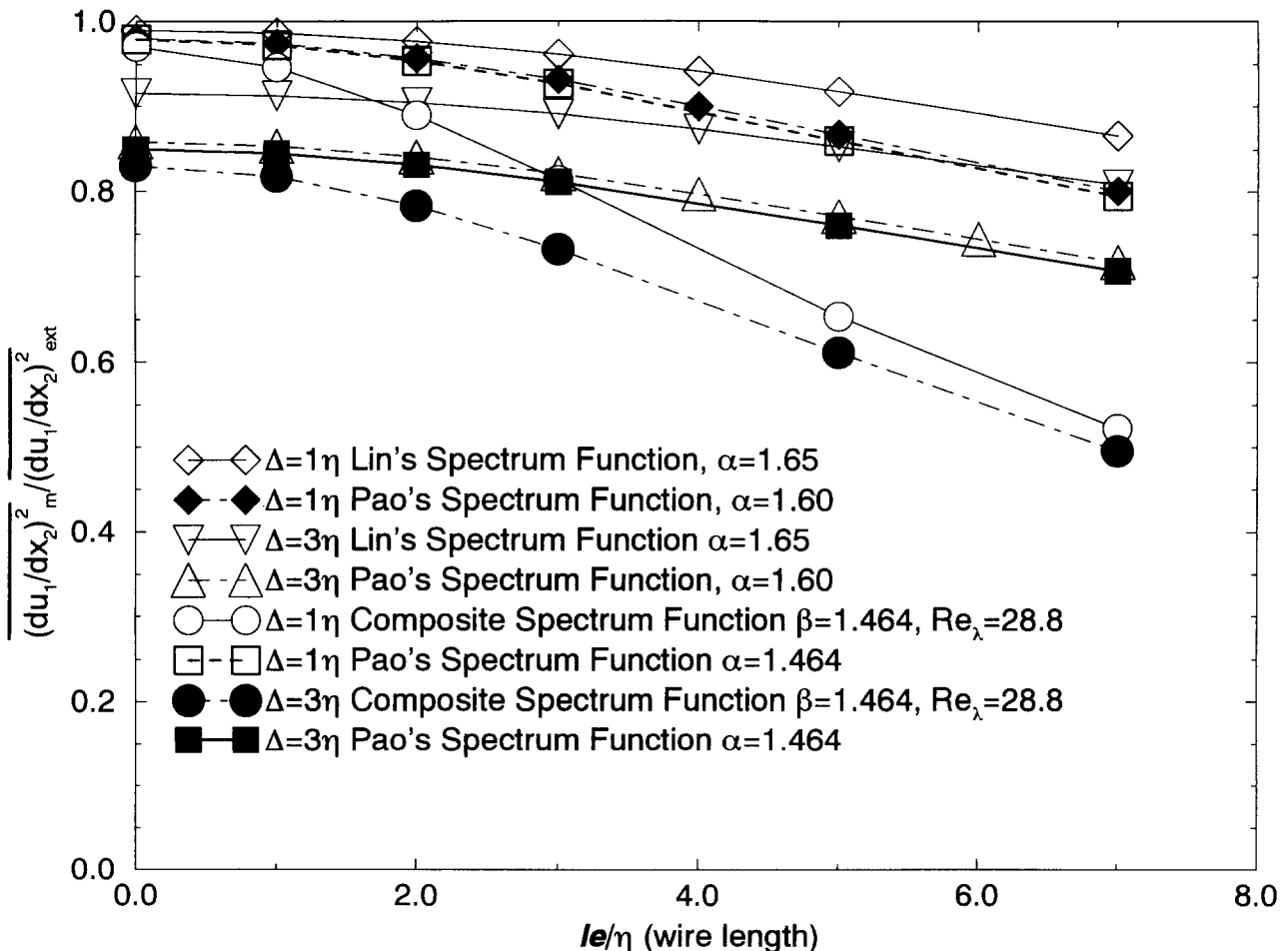


Figure 9. Attenuation of velocity derivative measurements due to finite-length wires in a parallel-wire probe with fixed separation distance.

where it is largest. It does have some effect; but the effect will not be as direct as that of the finite separation attenuation, which increases as the value of k_2 increases.

Figure 9 also illustrates the attenuation calculated for the composite spectrum function with $\text{Re} = 28.8$ and the attenuation that occurs in Pao's spectrum with $\alpha = 1.464$. It is clear that the addition of finite-length wires has a significant effect on the measured derivative. Although the separation distance is the critical dimension that determines the amount of attenuation if the wire separation distance and wire length are equal in magnitude, the wire length quickly becomes an important parameter if it is much larger than the wire separation.

TEMPERATURE DERIVATIVE MEASUREMENTS

The method for determining the attenuation of scalar derivative measurements follows a pattern similar to that of the velocity derivative calculations. Initially, the effect of the finite separation of two point wires is determined. This is followed by adding the effect of finite wire length. Comparisons are made for two spectral models.

Attenuation Due to Finite Separation

The derivation of the expression for the attenuation of measurements due to finite separation for the scalar field is similar to the derivation for the velocity field. The expression for the scalar derivative measurement is

$$\frac{[\theta(\mathbf{x}_a) - \theta(\mathbf{x}_b)]^2}{|\mathbf{x}_a - \mathbf{x}_b|^2} = \int \phi(\mathbf{k}) \frac{(2 - 2 \cos[\mathbf{k} \cdot (\mathbf{x}_a - \mathbf{x}_b)])}{|\mathbf{x}_a - \mathbf{x}_b|^2} d\mathbf{k}, \quad (25)$$

where ϕ is the scalar three-dimensional spectrum and the positions of the centers of each of the wires in the probe are \mathbf{x}_a and \mathbf{x}_b .

The equation for the exact derivative of the scalar field is given by [17]

$$\left(\frac{d\theta}{dx_\alpha} \right)^2 = \int (k_\alpha)^2 \phi(\mathbf{k}) d\mathbf{k}, \quad (26)$$

where α is used to indicate that there is no summation over the index. Since the scalar field is assumed to be isotropic in wavenumber space, the mean square exact derivative and the mean square measured derivatives are independent of the probe orientation in the field. It is possible to apply the mean square calculations for one separation direction to any separation direction, so the calculations are carried out for only one direction in this analysis. This obviously is not true for an anisotropic field.

As for the velocity derivative measurements above, it is possible to Taylor expand the term multiplying the three-dimensional spectrum in Eq. (25) and note that the first term of this expansion multiplied by the three-dimensional spectrum is equal to the exact derivative in Eq. (26). If the separation distance is in the x_2 direction, the expansion of the term is the same as for the velocity derivative [see Eq. (7)]. Therefore, the equations for the

exact and measured derivatives of the scalar are equal in the limit of zero separation.

Temperature Spectrum

The three-dimensional spectrum of the scalar quantity ϕ is the three-dimensional Fourier transform of the scalar correlation function in a homogeneous field; that is,

$$\phi(\mathbf{k}) = \frac{1}{8\pi^3} \int \overline{\theta(\mathbf{x})\theta(\mathbf{x} + \mathbf{r})} e^{i(\mathbf{k} \cdot \mathbf{r})} d\mathbf{r}, \quad (27)$$

where θ represents a scalar quantity, temperature in this analysis. It is possible to define the three-dimensional spectrum as a function of a scalar spectrum function, $E_\theta(k)$, using the relationship given by

$$E_\theta(k) = \int \phi(\mathbf{k}) d\sigma(k), \quad (28)$$

where the integration is carried out over spherical shells of radius k in wave space. For isotropic turbulence, the three-dimensional spectrum is related to E_θ by

$$\phi(\mathbf{k}) = E_\theta(k)/4\pi k^2. \quad (29)$$

The previous work (e.g., Wyngaard [2]) used Corrsin's [10] spectrum function

$$\tilde{E}_\theta(\tilde{k}) = \alpha_\theta \tilde{k}^{-5/3} \exp\left[-\frac{3}{2}\left(\frac{\alpha_\theta}{\text{Pr}}\right)\tilde{k}^{4/3}\right] \quad (30)$$

in the definition of the three-dimensional spectrum, where $\tilde{E}_\theta(\tilde{k}) = E_\theta(k)(\varepsilon^{1/3}/\varepsilon_\theta \eta^{5/3})$ is the nondimensional scalar spectrum function. In this study the value of the Prandtl number is 0.72 (air) and the value of α_θ is chosen as 0.66 to be consistent with the range of values reported by Champange et al. [23]. (A derivation of the relationship between α_θ and the one-dimensional constant reported by Champange et al. [23] is included in Appendix II.)

Like Pao's spectrum function for the velocity, Corrsin's scalar spectrum function is also physically unrealistic in the high-wavenumber region, and it has a tendency to overestimate the spectrum function in this region. A second spectrum function suggested by Hill [13] is used in the analysis. This function, which rolls off faster in the high-wavenumber region, is given by

$$\tilde{E}_\theta(\tilde{k}) = \alpha_\theta (\tilde{k}^{-5/3} + Q\tilde{k}^{-1}) \exp\left[-\frac{\alpha_\theta}{\text{Pr}}\left(\frac{3}{2}\tilde{k}^{4/3} + Q\tilde{k}^2\right)\right]. \quad (31)$$

Q is 2.50 as suggested by Hill [13], while α_θ and Pr are the same as above.

The spectrum functions for the two different models are illustrated in Fig. 10, which illustrates that Hill's spectrum function rolls off significantly faster than Corrsin's spectrum function in the high-wavenumber region. As for the velocity, the spectrum that the experimenter measures is the one-dimensional scalar spectrum defined as

$$F_{\theta\theta}^1 = \int \int \phi(\mathbf{k}) dk_2 dk_3. \quad (32)$$

The one-dimensional spectrum $\tilde{F}_{\theta\theta}^1 = F_{\theta\theta}^1(\varepsilon^{1/3}/\varepsilon_\theta \eta^{5/3})$ for each of the models is shown in Fig. 11. The spectra shown in this figure are the positive-wavenumber portion of the whole-line spectrum.

Attenuation of the Mean Square Derivative Measurements

Figure 12 shows how the normalized measured derivative varies with the separation distance of the wires. It is evident that the error introduced into the derivative measurements by spatial filtering increases with separation distance. In addition, there is significantly less attenuation for Hill's spectrum than for Corrsin's spectrum. Therefore, the amount of attenuation that occurs is dependent on the shape of the spectrum at the high wavenumbers, and the sensitivity increases with separation distance. The error in the measured mean square derivative calculated using Hill's spectrum is 10% when the separation distance between the wires is approximately 3 times the Kolmogorov length scale.

Interpreting One-Dimensional Spectra

The interpretation of the measured one-dimensional derivative, illustrated in Fig. 13, has many of the same problems discussed in the previous section on velocity measurements, so an extended discussion is not included here. The key problem still exists for these spectra in the sense that the measured one-dimensional spectrum is a

sum of entities that have been attenuated by different amounts (if the separation is not in the x_1 direction), so that it is not possible to characterize a cutoff frequency using the one-dimensional spectra without knowledge of the three-dimensional spectrum that is being measured.

Attenuation Due to Finite Length

The expression for the attenuation due to finite length and finite separation distance for the temperature spectrum is

$$\begin{aligned} & \frac{[\theta(\mathbf{x}_a) - \theta(\mathbf{x}_b)]^2}{|\mathbf{x}_a - \mathbf{x}_b|^2} \\ &= \frac{1}{|\mathbf{x}_a - \mathbf{x}_b|^2} \int \phi(\mathbf{k}) \{2 - 2 \cos[\mathbf{k} \cdot (\mathbf{x}_a - \mathbf{x}_b)]\} \\ & \quad \times \left(\frac{\sin(k \cdot l/2)}{k \cdot l/2} \right)^2 dk. \end{aligned} \quad (33)$$

Figure 14 shows the attenuation of the mean square measured derivatives for probes with wires of finite length and finite separation distances of 1 and 3 Kolmogorov lengths. The error in the measurement is dependent on

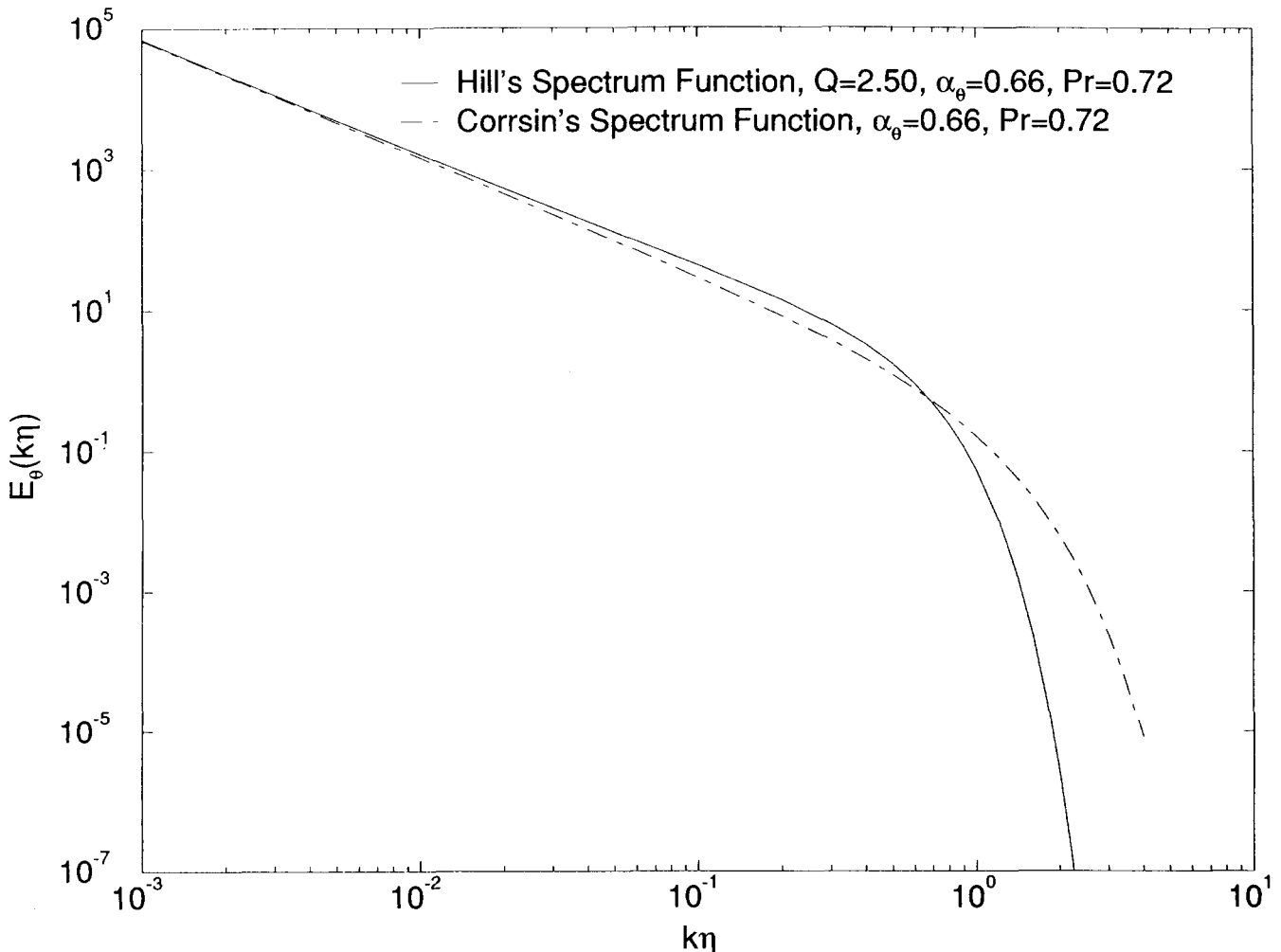


Figure 10. Temperature spectrum functions used to model the three-dimensional spectrum of a passive scalar.

which spectral model is used, with Corrsin's spectrum giving the larger error. The additional error introduced by wire with a length of 3–4 times the Kolmogorov length scale is less than 2–3%. Similar to the velocity derivative measurements, the separation distance is the more critical dimension if the wire length and wire separation are of comparable magnitude.

PRACTICAL CONSIDERATIONS

The spatial attenuation introduced by the probe is not the only consideration in derivative measurements, and there are several other issues that must be considered when the analysis in this paper is applied to experimental design or to interpreting experimental data. A brief review of some of these issues is included for completeness (relevant references are given for further discussions of the issues).

Noise

There is without question a potential downside to the reduction in separation distance. Each of the measured velocity signals will have electronic and quantization noise. Therefore each of the measured velocities can be represented as the sum of the velocity determined by the hot

wire and a noise term

$$u_1^e(x_a) = u_1(x_a) + n_a, \quad u_1^e(x_b) = u_1(x_b) + n_b, \quad (34)$$

where u^e is the total measured signal and u is the signal measured by the transducer. Each of the signals has a separate component of noise represented by n_a and n_b .

The entire signal with the noise included must be used to approximate the mean square derivative in the difference equation. Therefore,

$$\overline{\left(\frac{\partial u_1}{\partial x_2} \right)_m^2} = \frac{[u_1^e(x_a) - u_1^e(x_b)]^2}{|x_a - x_b|^2}. \quad (35)$$

Inserting the definitions from Eq. (34) into Eq. (35) implies that the measured derivative in a real experiment is

$$\begin{aligned} & \frac{[u_1(x_a) + n_a - (u_1(x_b) + n_b)]^2}{|x_a - x_b|^2} \\ &= \frac{[u_1(x_a) - u_1(x_b)]^2}{|x_a - x_b|^2} + \frac{n_a^2 + n_b^2 - 2n_a n_b}{|x_a - x_b|^2}, \end{aligned} \quad (36)$$

assuming that the velocity measured by the transducer and the noise are uncorrelated [if this isn't true, there are

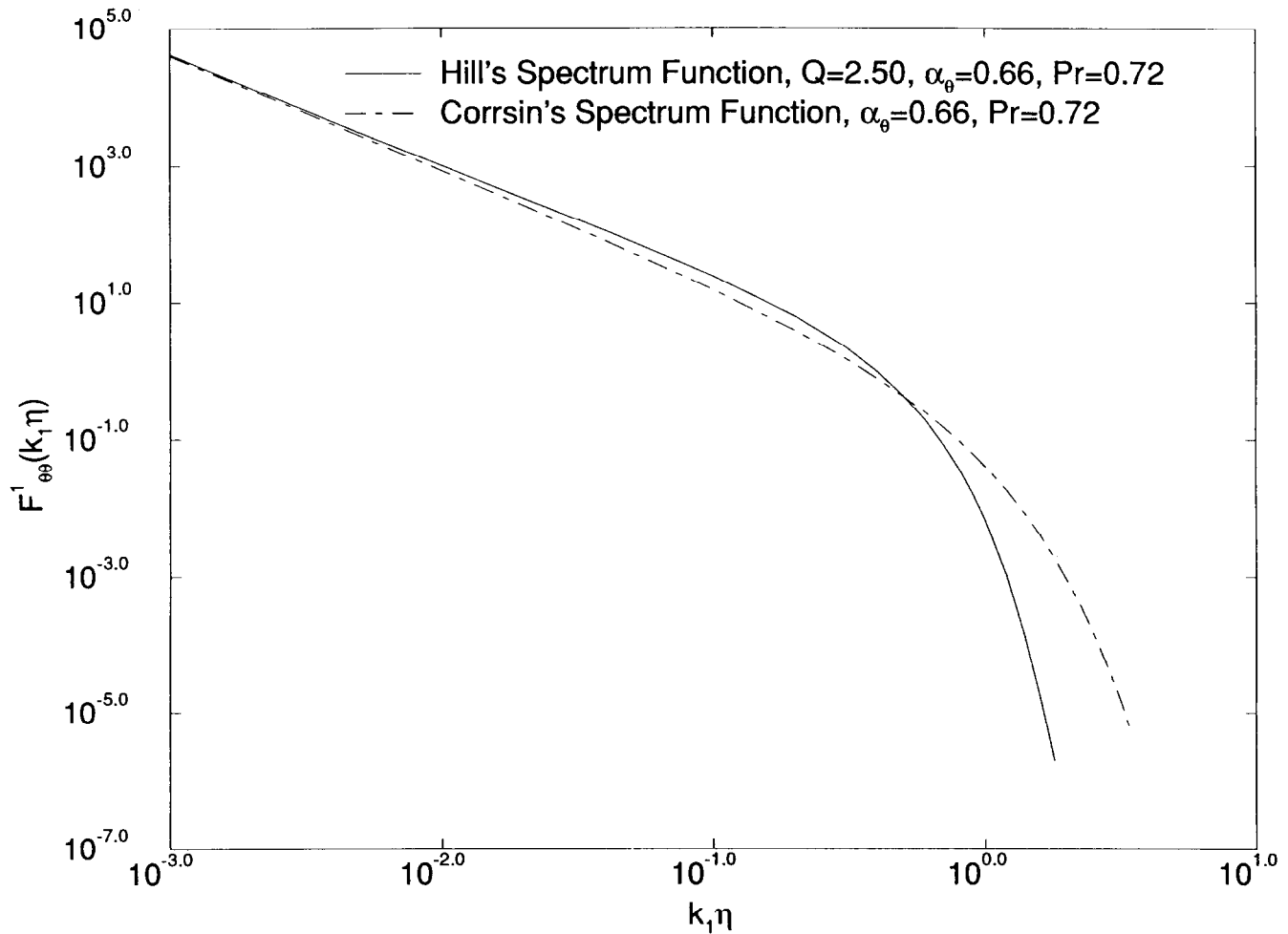


Figure 11. Comparison of the one-dimensional temperature spectra.

additional terms in Eq. (36)]. The first term on the right-hand side of Eq. (36) is the difference equation written for the velocity measured by the transducer. This is the quantity called the measured mean square derivative in the previous sections. If the noise from the two lines is not correlated or only partially correlated, the numerator of the noise term will be finite for all separation distances. As the separation distance approaches zero, the first term on the right-hand side approaches the true derivative at the point, while the second term becomes infinity. To ensure that the total measured quantity estimates the velocity or temperature derivative and not the noise, the mean square value of the velocity or temperature difference should be kept much larger than the mean square noise contribution.

Antonia et al. [3] documented the occurrence of this problem experimentally by plotting the left-hand side of Eq. (36) versus the separation distance. It was clearly evident that the measured derivative approaches infinity as the separation distance approaches zero; however, it was possible to extrapolate to obtain an estimate of the first term on the right-hand side. When such an extrapolation is not carried out, a minimum separation distance for the hot wires must be determined for an experimental setup. The magnitude of this distance is totally dependent

on the quantity of noise in the experimental setup and should be determined experimentally for each setup. Further discussion of this topic can be found in Subramanian et al. [24] and Klewicki and Falco [22].

Relating Measurements at Different Positions in a Flow

It is clear from the analysis of the velocity derivative measurements that the attenuation that occurs in the measurement of the derivative is dependent on the Reynolds number of the turbulence that is being measured. This is an important factor that must be taken into account when measurements from two locations are compared, but there are other important factors that must be considered when measurements at different locations are considered.

First, the attenuation of derivative measurements is dependent on the size of the probe relative to the flow, not just the size of the probe. Normally the probe size is fixed, but the Kolmogorov length scale of the flow can change between positions in the flow even if the characteristic length scale of the energy containing eddies is not different. This would occur if the Reynolds numbers of the flow at the two positions were different. This would cause the attenuation to be different at the two positions,

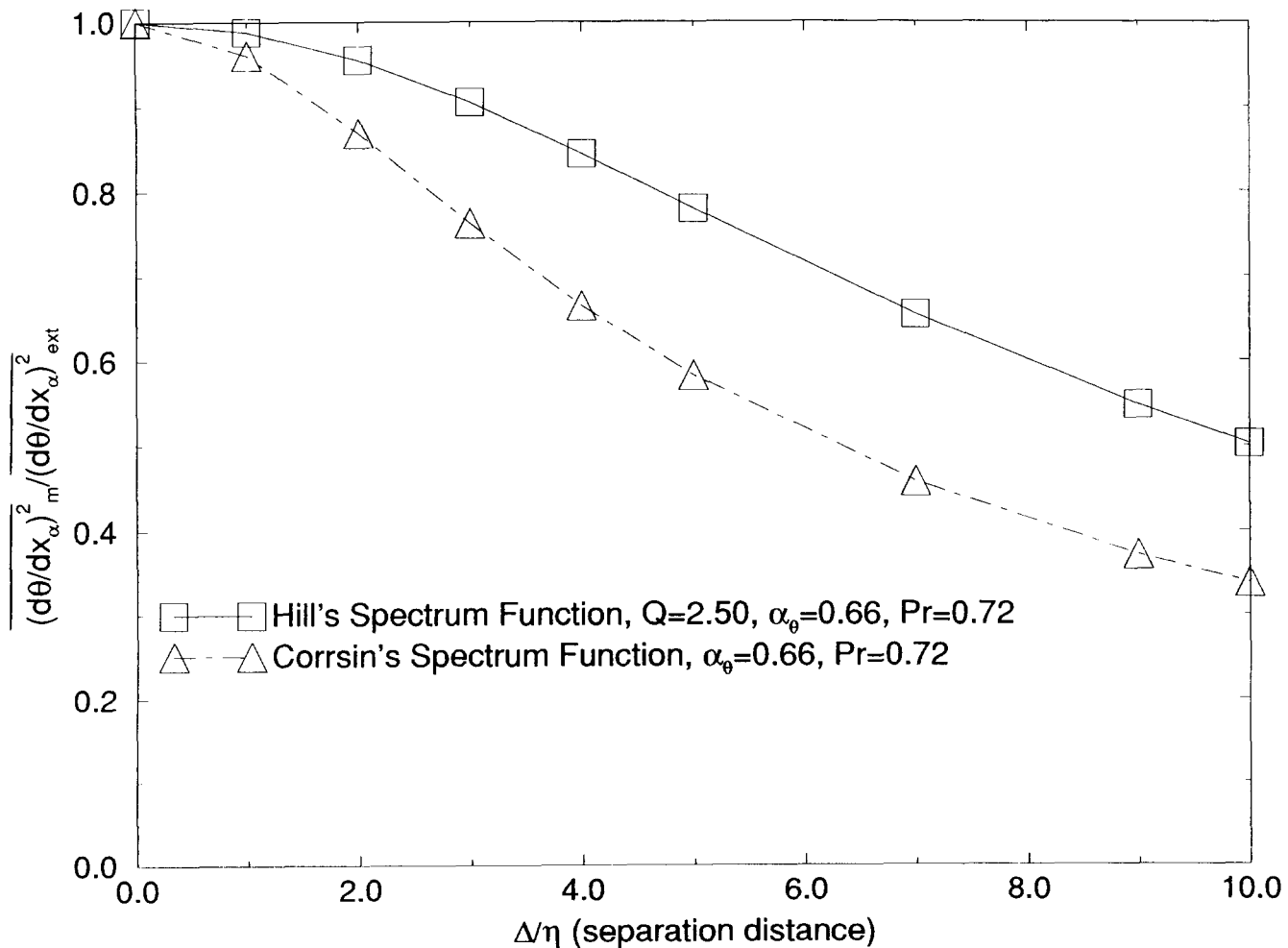


Figure 12. Attenuation of the temperature derivative measurements due to the finite separation of zero-length parallel wires.

that is,

$$\Delta = \text{fixed},$$

$$\eta = f(Re) \Rightarrow \text{attenuation} = h\left(\frac{\Delta}{\eta}\right) = g(Re). \quad (37)$$

This effect is distinct from the Reynolds number effect discussed earlier and can occur even at high Reynolds numbers. This has been discussed for the case of boundary layer flows in several papers (see, e.g., [11, 25]). It is also possible for the Kolmogorov length scale to vary in a constant Reynolds number flow such as the far field of the axisymmetric jet, where all of the length scales grow approximately linearly with streamwise position. This effectively reduces the size of the probe relative to the turbulence that is being measured as the probe is moved downstream, thereby reducing the amount of attenuation that occurs in the measurement.

Second, if the probe is used in flow where the anisotropy of the three-dimensional spectrum varies between points, it is quite possible that the amount of attenuation occurring in derivative measurements could also vary. Since the finite dimensions of the geometry filter the three-dimensional spectrum in specific directions, variations in the anisotropy relative to these particular directions will cause

variations in the normalized attenuation. This problem may be especially prevalent in low Reynolds number flows without a significant cascade, since the small-scale motions are more likely to be anisotropic and the large nonhomogeneous scales may contribute to the derivative measurement.

Data Correction

We do not recommend the use of the analysis in this paper for data correction, since the analysis is carried out using assumed forms of the three-dimensional spectrum of the turbulence. Determination of the correction factor for a particular experiment requires first obtaining the three-dimensional spectrum, which is generally impossible. The only method presently available uses isotropic spectrum relationships to generate a three-dimensional spectrum from the measured one-dimensional spectrum, but this assumes that the turbulence spectrum in the region of interest is isotropic. Moreover, it also assumed that an unfiltered one-dimensional spectrum is available, which is never true. If, in fact, this method could be used to generate a three-dimensional spectrum for the turbulence, then there is no point in doing the experiment because all of the derivatives could be calculated from it.

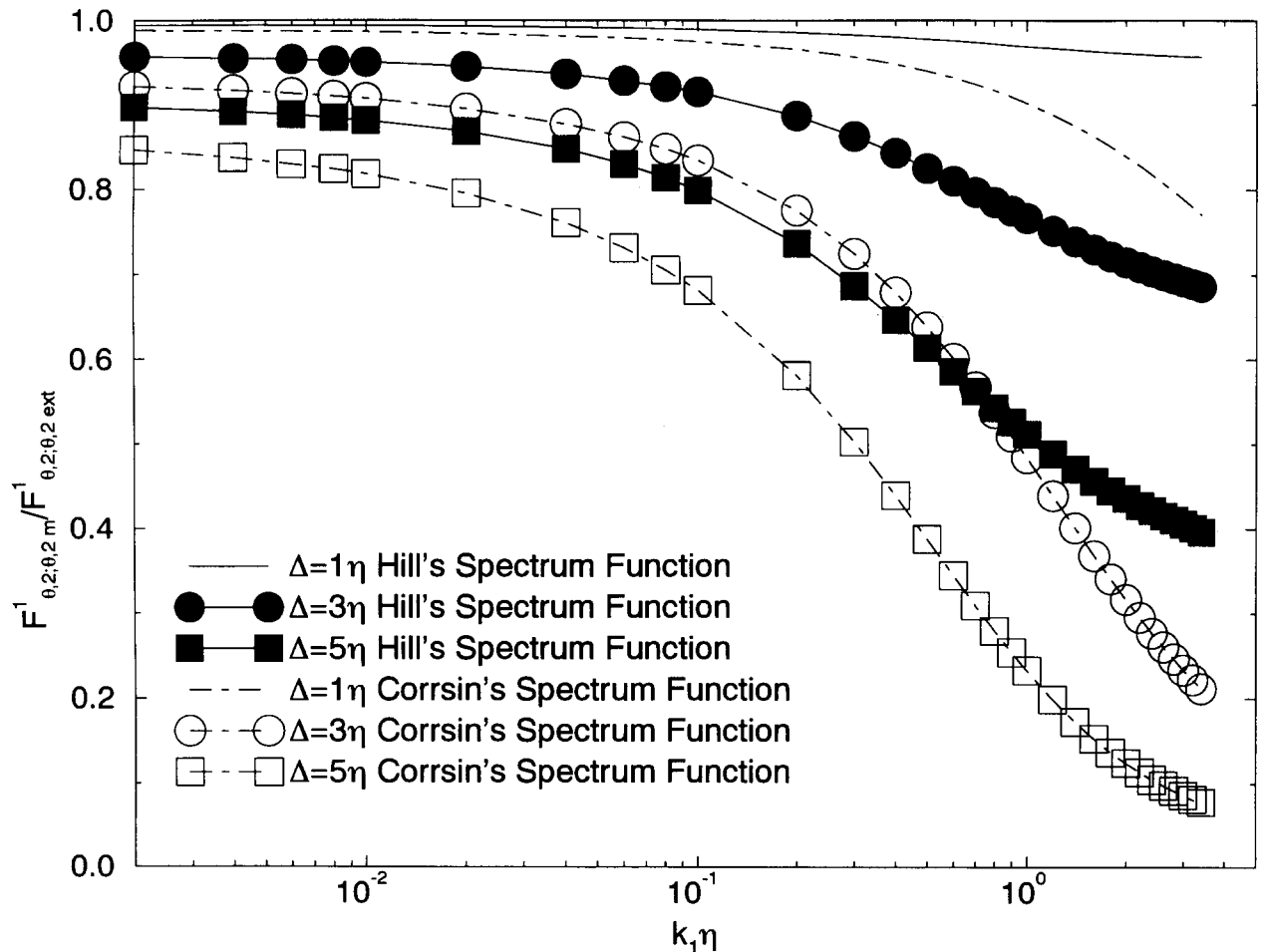


Figure 13. Normalized attenuation of the one-dimensional temperature derivative spectra measured by finitely separated zero-length parallel wires.

It should also be noted that the analysis in this paper considered only isotropic turbulence, so it is not possible to determine the effect local anisotropy has on the attenuation of derivative measurements. Therefore, the analysis in the current paper can be used only as an indication of the magnitude of the error in these cases as opposed to an absolute measure. This is especially true if the experiment is at a relatively low Reynolds number.

PRACTICAL USEFULNESS / SIGNIFICANCE

The information included in this paper is useful for the design phase of an experiment to ensure that the sizes of the hot-wire probes used in the experiment are compatible with the scales of the flow being measured. If they are not, the design of the experiment can be altered to ensure that the estimate of the error is reasonable, or the experiment can be abandoned entirely. The techniques outlined in this paper only allow the derivation of attenuation equations for homogeneous turbulence assuming that Taylor's frozen field hypothesis is exact. However, even this restrictive model, if properly interpreted, gives the experimentalist an intelligent starting point in understanding how spatial attenuation affects the measurement of

nonhomogeneous turbulence and a valuable analytical tool in experimental design.

CONCLUSIONS AND DISCUSSION

It is evident that the finite wire separation distance and finite wire length in the parallel-wire probe cause significant attenuation of measured velocity derivatives. The curves generated from Lin's and Hill's spectrum models offer a realistic estimate of the spatial attenuation error in the derivative measurements. A comparison of the measurements for Pao's and Lin's or Corrsin's and Hill's spectrum functions indicate that the error in the measurements introduced by spatial filtering is quite sensitive to the shape of the spectrum at high wavenumbers. An examination of the results calculated with the composite spectrum function indicates that the attenuation is also sensitive to the model of the low-wavenumber region for low Reynolds number turbulence, and this effect can significantly enhance the amount of error that occurs. In addition, the sensitivity of the error to the shape of the spectrum increases as the separation distance between the wires increases. Therefore, increasing the relative separation distances not only increases the error introduced by

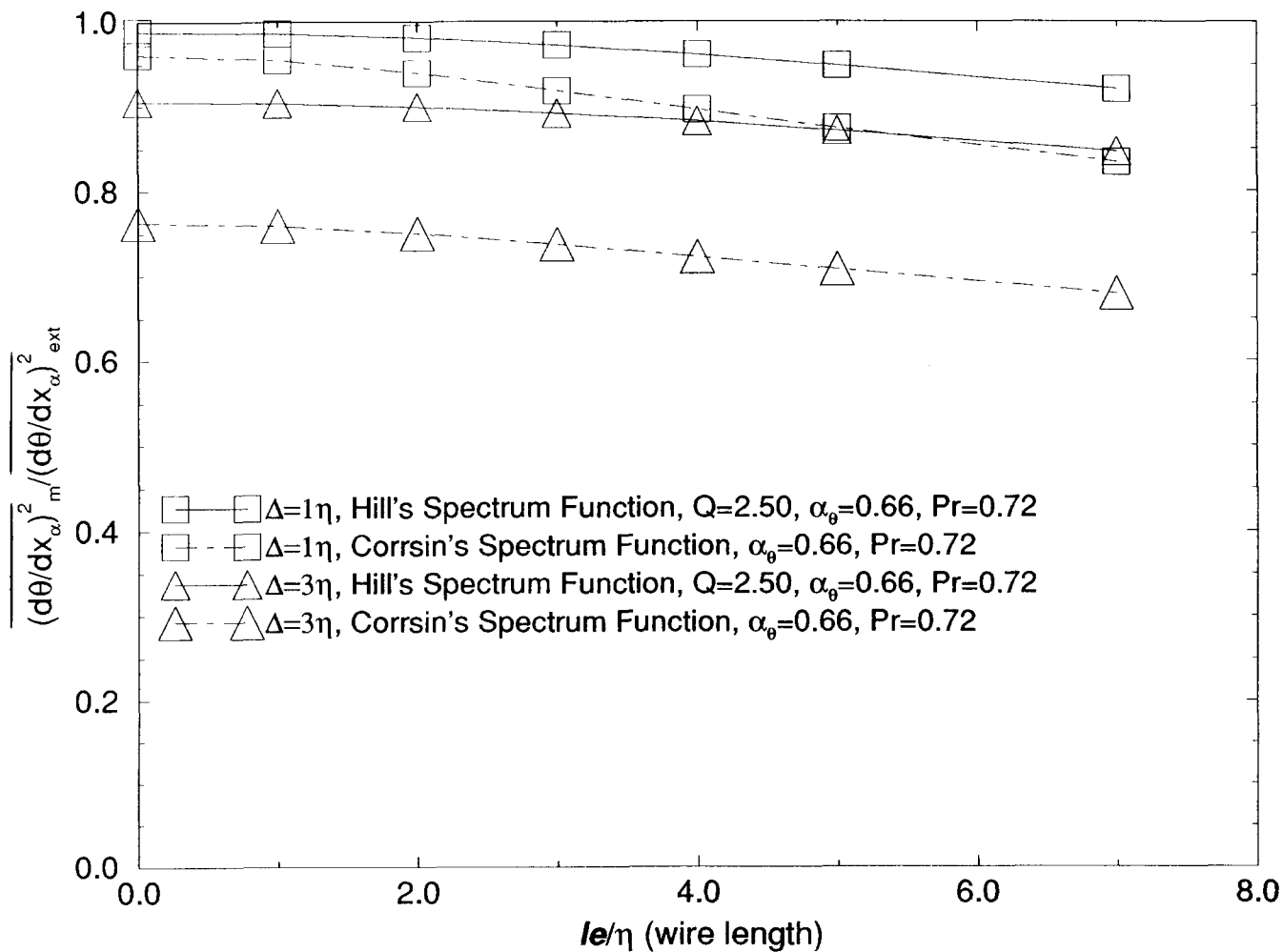


Figure 14. Attenuation of temperature derivative measurements due to the finite-length wires in a parallel-wire probe with fixed wire separation distance.

the parallel hot wire, it also increases the uncertainty about the quantity of error. Since the uncertainty in the magnitude of the error increases as error increases, it is suggested that postprocessing is not a suitable manner of handling the spatial attenuation problem.

For all of the spectral models, the effect of finite wire length introduces a smaller error into the calculation of the derivatives than the finite separation for a parallel-wire probe if the wire length and wire separation distance are of comparable magnitude and normal. In the case of low Re flow, the rolloff due to the finite wire length was more significant than in the high models, indicating that the effect of the finite wire length becomes more significant for smaller ratios of wire length and separation distances when the measurements are made in a flow with a small turbulence Reynolds number.

At small separation distances, measurements of the derivative can be overwhelmed by the noise in the experimental setup. The distance at which this occurs will differ from setup to setup and should be determined experimentally. In addition, a hot-wire probe with fixed dimensions will attenuate derivative measurements at two locations by different amounts if the Kolmogorov length scale is different at the two points. The analysis in this paper indicates a need for careful experimental design and should not be used as a substitute for a careful study of the errors described. It is also clear from the analysis in this paper that one-dimensional spectrum measurements are a poor tool for carrying out this analysis.

RECOMMENDATIONS

The work outlined in this paper is valuable for assessing the attenuation introduced by a parallel-wire probe, but it does not automatically follow that the size limitations for the parallel-wire probe will apply to other multiwire probes. It is necessary to examine each probe to determine its characteristics. Two of the authors of the present paper have extended the analysis to probes that use two cross wires to measure four components of the derivative and a nine-wire vorticity probe.¹ A number of other investigations are included in the references. Experimentalists using probes that have not been investigated should carry out either an analytical or an experimental investigation of their probe.

We thank J. Citriniti for his suggestions and assistance in editing the manuscript.

APPENDIX I

The composite spectrum suggested by Hellend et al. [14] is a product of von Karman's [20] empirical spectrum function for the low-wavenumber region and Pao's [9] spectrum function for the high-wavenumber region. These two spectrum functions are infinite Reynolds number models of the large-scale and small-scale motions, respectively, so neither includes a realistic model of the full range that occurs in any finite Reynolds number flow. The product of

the two models, given by

$$E(k) = \alpha \varepsilon^{2/3} L^{5/3} \frac{(kL)^4}{[1 + (kL)^2]^{17/6}} \exp\left[-\frac{3}{2} \beta (k\eta)^{4/3}\right], \quad (\text{AI.1})$$

models both regions. The constant α is Kolmogorov's constant and is defined as 1.6 in this study.

To ensure that $E(k)$ is a proper spectrum function, it is important to ensure that it satisfies the relationship between the dissipation per unit mass, ε , and $E(k)$ for isotropic turbulence, which is given by [18]

$$\varepsilon = 2\nu \int_0^\infty k^2 E dk. \quad (\text{AI.2})$$

Substituting Eq. (AI.1) into Eq. (AI.2) and performing a change of variable to $\tilde{k} = k\eta$ (noting that $\varepsilon^{1/3} = \nu/\eta^{4/3}$ from the definition of η), this yields

$$1 = 2\alpha \int_0^\infty \frac{\tilde{k}^6}{[(\eta/L)^2 + \tilde{k}^2]^{17/6}} \exp\left[-\frac{3}{2} \beta(\tilde{k})^{4/3}\right] d\tilde{k}. \quad (\text{AI.3})$$

Therefore, the model parameter β is determined for a given choice of L/η by satisfying Eq. (AI.3).

The turbulence Reynolds number of the spectrum function can be characterized by the turbulence Reynolds number base on the Taylor microscale,

$$\text{Re}_\lambda = u\lambda/\nu, \quad (\text{AI.4})$$

where $u^2 = \overline{(u_i u_i)}/3$. For isotropic turbulence the Taylor microscale is given by [18]

$$\lambda^2 = 15\nu u^2/\varepsilon. \quad (\text{AI.5})$$

This expression can be related to the three-dimensional spectrum of the turbulence, $E(k)$, by using the relationship

$$\frac{3}{2} \overline{u_i u_i} = \int_0^\infty E(k) dk. \quad (\text{AI.6})$$

Thus,

$$\text{Re}_\lambda = \left(\frac{20}{3}\right)^{1/2} \int_0^\infty E(\tilde{k}) d\tilde{k}, \quad (\text{AI.7})$$

where $\tilde{k} = k\eta$. The values of L/η , β , and Re_λ for the spectrum functions used in this analysis are included in Table 1.

APPENDIX II

To ensure that the model constants for the scalar models are consistent with the constants reported in the literature, it is necessary to compare the definitions used to define the constants. For example, Champagne et al. [23] indicate that the value of the Kolmogorov constant for the one-dimensional half-line spectrum, β_θ ,

$$F_{11}^{1*} = \beta_\theta \varepsilon_\theta \varepsilon^{-1/3} k_1^{-5/3}, \quad \overline{\theta^2} = \int_0^\infty F_{\theta\theta}^{1*}(k_1) dk_1, \quad (\text{AII.1})$$

is approximately 0.4. The asterisk is used to distinguish the half-line spectrum from the whole-line spectrum $F_{\theta\theta}^1$

¹This analysis will be included in a future publication.

used in this paper. The relationship between the whole-line and half-line one-dimensional spectra follows from the fact that the whole-line one-dimensional spectrum is real and even. Thus,

$$\overline{\theta^2} = \int_{-\infty}^{\infty} F_{\theta\theta}^1(k_1) dk_1 = 2 \int_0^{\infty} F_{\theta\theta}^1(k_1) dk_1. \quad (\text{AII.2a})$$

Therefore,

$$2F_{\theta\theta}^1(k_1) = F_{\theta\theta}^{1*}(k_1). \quad (\text{AII.2b})$$

In this analysis, the three-dimensional spectrum function $E_\theta(k)$ is defined such that

$$\overline{\theta^2} = \int_0^{\infty} E_\theta(k) dk, \quad (\text{AII.3a})$$

where

$$E_\theta(k) = \iint_{|k|=k} \phi(\mathbf{k}) d\sigma(\mathbf{k}), \quad (\text{AII.3b})$$

where $E_\theta(k)$ is the energy of spherical shells of radius k .

The three-dimensional spectrum function $\phi(\mathbf{k})$ of an isotropic scalar quantity θ is only a function of the magnitude of the wavenumber vector k (see Appendix 4 of Lumley [15]), so it is possible to write the three-dimensional spectrum function as

$$\phi(\mathbf{k}) = A(k). \quad (\text{AII.4})$$

Substituting the equation of the three-dimensional spectrum, Eq. (AII.4), into the second equation in (AII.3) and transforming to a spherical coordinate system, so $d\sigma(\mathbf{k}) = k^2 \sin \xi d\varphi d\xi$ (ξ is used in place of the more traditional angle θ to avoid confusion), leads to the expression

$$E_\theta(k) = \int_{-\pi}^{\pi} \int_0^{2\pi} A(k) k^2 \sin \zeta d\varphi d\zeta = 4\pi k^2 A(k). \quad (\text{AII.5a})$$

Therefore,

$$A(k) = \frac{E_\theta(k)}{4\pi k^2}. \quad (\text{AII.5b})$$

The definition of the whole-line one-dimensional spectrum is

$$\begin{aligned} F_{\theta\theta}^1(k_1) &= \iint_{-\infty}^{\infty} \phi(\mathbf{k}) dk_2 dk_3 \\ &= \int_0^{2\pi} \int_0^{\infty} \frac{E_\theta[(\sigma^2 + k_1^2)^{1/2}]}{4\pi k^2} \sigma d\theta d\sigma \\ &= \frac{1}{2} \int_{k_1}^{\infty} \frac{E_\theta(k)}{k} dk, \end{aligned} \quad (\text{AII.6})$$

where the first coordinate transformation is to polar coordinates on the $k_2 k_3$ plane and the second is a transformation to a new variable k that is equal to $(\sigma^2 + k_1^2)^{1/2}$, where k_1 is a constant. Finally, to determine the Kolmogorov constant for the three-dimensional spectrum, the function $E_\theta(k)$ is assumed to be of the form

$$E_\theta(k) = \alpha_\theta \varepsilon_\theta \varepsilon^{-1/3} k^{-5/3}. \quad (\text{AII.7})$$

Substituting this into Eq. (AII.6) and integrating yields

$$F_{\theta\theta}^1(k_1) = \frac{3}{10} \alpha_\theta \varepsilon_\theta \varepsilon^{-1/3} k_1^{-5/3}. \quad (\text{AII.8})$$

Equations (AII.1), (AII.2), and (AII.8) yield a relationship between the Kolmogorov constant for the three-dimensionalized spectrum function α and the Kolmogorov constant for the half-line one-dimensional spectrum β_θ ; that is,

$$2F_{\theta\theta}^1(k_1) = \frac{3}{5} \alpha_\theta \varepsilon_\theta \varepsilon^{-1/3} k_1^{-5/3} = F_{11}^{1*} = \beta_\theta \varepsilon_\theta \varepsilon^{-1/3} k_1^{-5/3}, \quad (\text{AII.9a})$$

so

$$\alpha_\theta = \frac{5}{3} \beta_\theta. \quad (\text{AII.9b})$$

Therefore α_θ is set equal to 0.66 in the current analysis.

It should be noted that there is only one value of α_θ that is the proper Kolmogorov constant of the isotropic model, but depending on exactly which definitions are chosen it is possible to get several different values of the one-dimensional constant. For example, the one-dimensional constant for the whole-line spectrum is half of the constant determined using the half-line spectrum.

NOMENCLATURE

$E(\)$	velocity energy spectrum, $(\text{m/s})^2 \text{ m}$
$E_\theta(\)$	temperature energy spectrum, $K^2 \text{ m}$
\tilde{E}_θ	temperature spectrum function $(= E_\theta \varepsilon^{1/3} / \varepsilon_\theta \eta^{5/3})$, dimensionless
F_{11}^1	one-dimensional velocity spectrum, $(\text{m/s})^2 \text{ m}$
\tilde{F}_{11}^1	one-dimensional velocity spectrum $(= F_{11}^1 / u_k^2 \eta)$, dimensionless
$F_{1,2,1,2}^1$	one-dimensional spectrum of the derivative $(\partial u_1 / \partial x_2)^2$, m/s^2
$F_{\theta\theta}^1$	whole-line one-dimensional temperature spectrum, $K^2 \text{ m}$
$F_{\theta\theta}^{1*}$	half-line one-dimensional temperature spectrum, $K^2 \text{ m}$
$\tilde{F}_{\theta\theta}^1$	one-dimensional temperature spectrum $[= F_{\theta\theta}^1 (\varepsilon^{1/3} / \varepsilon_\theta \eta^{5/3})]$, dimensionless
\mathbf{k}	wavenumber vector in Fourier space, m^{-1}
k	magnitude of the wavenumber in Fourier space, m^{-1}
\tilde{k}	magnitude of the wavenumber in Fourier space $(= k \eta)$, dimensionless
k_1, k_2, k_3	the three components of the wavenumber vector in Fourier space, m^{-1}
L	characteristic length scale of the energy-containing eddies, m
\mathbf{l}	vector along the two wires relative to the center position of each wire, m
l	length scale of the turbulence defined by the relationship $\varepsilon = u^3/l$, m
l_e	length of the each wire in the probe, m
n	noise component of the measured signal after conversion to a velocity signal, m/s
Pr	Prandtl number ($= \nu/\alpha$), dimensionless
Q	constant included in Hill's energy spectrum, dimensionless
Re_λ	turbulence Reynolds number based on the Taylor microscale ($= u \lambda / \nu$), dimensionless

r	separation vector between two points, m
s	parameter variable along the wire, m
U	means convection velocity, m/s
u	turbulent velocity vector, m/s
u	$u^2 = (u_i u_i)/3$, m/s
u_1, u_2, u_3	three components of the velocity vector, m/s
$u_e()$	component of fluctuating streamwise velocity plus the experimental noise, m/s
$\hat{u}()$	Fourier coefficients of the streamwise fluctuating velocity, m^4/s
$\bar{u}()$	streamwise fluctuating velocity averaged along the length of the wires, m/s
u_k	Kolmogorov velocity [$= (\nu \epsilon)^{1/4}$], m/s
u_τ	friction velocity in a boundary layer, m/s
x	vector position of an arbitrary point in physical space, m
x_1, x_2, x_3	the three components of the coordinate system in physical space, m
x_a	vector position of the center of upper wire in the parallel-wire probe, m
x_b	vector position of the center of lower wire in the parallel-wire probe, dimensionless
y	distance from the wall in a boundary layer, m
y^+	distance from the wall in a boundary layer ($= y u_\tau / \nu$), dimensionless

Greek Symbols

α	Kolmogorov constant energy spectrum, dimensionless
α_θ	Kolmogorov constant temperature spectrum, dimensionless
β_θ	one-dimensional Kolmogorov constant, dimensionless
Δ	magnitude of the separation vector between the center of the wires in the parallel-wire probe, m
$\delta()$	Kronecker delta
ε	dissipation of turbulent kinetic energy, m^2/s^3
ε_θ	turbulent temperature dissipation, K^2/s
Φ_{ij}	three-dimensional spectrum of the i, j component of velocity, $(m/s)^2 m^3$
ϕ	three-dimensional spectrum of the temperature, $K^2 m^3$
η	Kolmogorov length scale, m
λ	Taylor microscale, m
$\theta()$	temperature at a point, K

Subscripts

sext	indicates the exact value of a given quantity for the specified spectrum function
m	indicates a measured quantity

REFERENCES

1. Wyngaard, J. C., Measurement of Small-Scale Turbulence Structures with Hot Wires, *J. Sci. Instrum.* **1**, 1105–1108, 1968.
2. Wyngaard, J. C., Spatial Resolution of the Vorticity Meter and Other Hot-Wire Arrays, *J. Sci. Instrum.* **2**, 983–987, 1969.
3. Antonia, R. A., and Mi, J., Corrections for Velocity and Temperature Derivative in Turbulent Flows, *Exp. Fluids* **14**, 203–208, 1993.
4. Antonia, R. A., Zhu, Y., and Kim, J., On the Measurement of Lateral Velocity Derivatives in Turbulent Flows, *Exp. Fluids* **15**, 65–69, 1993.
5. Wyngaard, J. C., Spatial Resolution of a Resistance Temperature Sensor, *Phys. Fluids* **14**, 2052–2054, 1971.
6. Browne, L. W. B., Antonia, R. A., and Chambers, A. J., Effects of the Separation Between Cold Wires on the Spatial Derivatives of Temperature in a Turbulent Flow, *Boundary-Layer Meter.* **27**, 129–139, 1983.
7. Hussein, H. J., and George, W. K., Measurement of Small Scale Turbulence in an Axisymmetric Jet Using Moving Hot Wires, 7th Symp. Turbulent Shear Flows, Stanford Univ., Aug. 14–18, 1989.
8. Champagne, F. H., The Fine-Scale Structure of the Turbulent Velocity Field, *J. Fluid Mech.* **86**, 67–108, 1978.
9. Pao, Y.-H., Structure of Turbulent Velocity and Scalar Fields at Large Wave-numbers, *Phys. Fluids* **8**, 1063–1075, 1965.
10. Corrsin, S., Further Generalization of Onsager's Cascade Model for Turbulent Spectra, *Phys. Fluids* **7**, 1156–1159, 1964.
11. Ligrani, P. M., and Bradshaw, P., Spatial Resolution and Measurement of Turbulence in the Viscous Sublayer Using Subminiature Hot-Wire Probes, *Exp. Fluids* **5**, 407–417, 19--.
12. Lin, J., Velocity Spectrum of Locally Isotropic Turbulence in the Inertial and Dissipation Ranges, *Phys. Fluids* **15**, 205–207, 1972.
13. Hill, R. J., Models of the Scalar Spectrum for Turbulent Advection, *J. Fluid Mech.* **88**, 541–562, 1980.
14. Hellend, K. N., Van Atta, C. W., and Stegen, G. R., Spectral Energy Transfer in High Reynolds Number Turbulence, *J. Fluid Mech.* **70**, 337–359, 1977.
15. Lumley, J. L., *Stochastic Tools in Turbulence*, Academic, New York, 1970.
16. George, W. K., and Lumley, J. L., The Laser Doppler Velocimeter and Its Application to the Measurement of Turbulence, *J. Fluid Mech.* **60**(1), 321–336, 1973.
17. Monin, A. S., and Yaglom, A. M., *Statistical Fluid Mechanics*, Vol. 2, MIT Press, Cambridge, MA, 1975.
18. Batchelor, G. K., *The Theory of Homogeneous Turbulence*, Cambridge Univ. Press, Oxford, United Kingdom, 1953.
19. Driscoll, R. J., The Influence of Spectral Transfer and Molecular Diffusion on Turbulent Mixing and Combustion, Ph.D. Thesis, State University of New York at Buffalo, Buffalo, NY, 1982.
20. von Karman, T., Progress in the Statistical Theory of Turbulence, *Proc. Natl. Acad. Sci. USA* **34**, 530–539, 1948.
21. Tennekes, H., and Lumley, J. L., *A First Course in Turbulence*, MIT Press, Cambridge, MA, 1972.
22. Klewicki, J. C., and Falco, R. E., On Accurately Measuring Statistics Associated with Small-Scale Structure in Turbulent Boundary Layer Using Hot-Wire Probes, *J. Fluid Mech.* **219**, 119–142, 1990.
23. Champagne, F. H., Friehe, C. A., LaRue, J. C., and Wyngaard, J. C., Flux Measurements, Flux Estimation Techniques, and Fine-Scale Turbulence Measurements in the Unstable Surface Layer Over Land, *J. Atmos. Sci.* **34**, 551–530, 1977.
24. Subramanian, C. S., Kandola, B. S., and Bradshaw, P., IC Aeronaute. Rep. 85-01, 1985.
25. Blackwelder, R. F., and Haritonidis, J. H., Scaling of the Bursting Frequency in Turbulent Boundary Layers, *J. Fluid Mech.* **132**, 87–103, 1983.

Received July 26, 1993; Revised December 23, 1994